# D5.1: Climate Assessment Report (CAR)

Reference: CCI_LAKES2-0034-CAR

Issue 2.1.0

11 rue Hermès, Parc Technologique du Canal – 31520 Ramonville Saint-Agne, France
Tel +33 (0)5 61 39 47 00 Fax +33(0)5 61 75 10 14
www.cls.fr

## CHRONOLOGY ISSUES

| Revised Issue | Legacy issues | Date | Objective | Written/Checked by |
|---|---|---|---|---|
| 1.0 | 1.0 | 06/08/2020 | Draft | G. Free, C. Giardino, M. Pinardi, M. Bresciani |
| | 1.1 | 16/09/2020 | Revision following ESA review | G. Free, C. Giardino, M. Pinardi, M. Bresciani |
| | 2.0 | 30/07/2021 | Draft of version 2 | G. Free, C. Giardino, M. Pinardi, M. Bresciani |
| | 2.1 | 29/11/2021 | Revision following ESA review | G. Free |
| | 3.0 | 14/02/2022 | Changes in UC5 § 5.2.5 | Adriana Constantinescu |
| 2.02 | 2.0.2.0 | 15/11/2023 | Draft | Pinardi M., Giardino C., Caroni R., Amadori M., Tellina G., Bresciani M. (CNR) Jiang D., Spyrakos E., Jones I. (UoS) Scholze J., Stelzer K. (BC) |
| | 2.0.2.1 | 15/12/2023 | Internal review | Simis S. |
| | 2.0.2.2 | 31/01/2024 | Reviewed by ESA | Pinardi M. |
| 2.1.0 | 2.1.0 | 15/07/2025 | Draft | Pinardi M., Caroni R., Greife A.J., Amadori M., Bresciani M. Giardino C. (CNR)<br>Jiang D. (UoS)<br>Scholze J. (BC) |
| | 2.1.0 | 18/07/2025 | Internal review | Simis S. |

Note: versioning prior to 2023 did not follow the CRDP release sequence. The revised versioning in the first column should be used for future consistency. The versioning of the CAR follows the version of CRDP that is described. In this document the version v2.1.0 of the CRDP is analysed.

| | | |
|---|---|---|
| **Checked by** | Stefan Simis - PML | S. Simis |
| **Approved by** | Philippe Mourot - CLS | Pmourot |
| **Authorized by** | Clément Albergel - ESA | clement.albergel |

## BIBLIOGRAPHIC REFERENCE

This document may be cited as:

Pinardi M., Caroni R., Greife A.J., Amadori M., Bresciani M., Giardino C., Jiang D., Scholze J., 2025. Climate Assessment Report (CAR), version 2.1.0. European Space Agency.

## LIST OF CONTENTS

# 1 Executive summary

Lakes provide essential aquatic ecosystem services, storing about 87% of liquid surface freshwater on Earth (Messager et al., 2016). However, lake ecosystems are under severe threat worldwide from anthropogenic pressures including climate change. Lakes play an essential role in local and global climate regulation, and they integrate responses to changes in their catchments over time. Since in situ observations of lake proprieties are relatively scarce and unevenly distributed both locally and globally, the use of satellite-derived products can expand and complement measurements across spatial and temporal scales.

In this context, 2024 inland water bodies have been selected for long-term observation records of the Lakes Essential Climate Variables (ECVs), within the European Space Agency (ESA) Climate Change Initiative (CCI), a global monitoring programme aiming to fulfil long-term satellite-based product requirements for climate modelling and observation, set by the Global Climate Observation System (GCOS).

The overarching objective of the Lakes_cci project is to produce and validate a consistent dataset of the thematic variables grouped under the Lakes ECV: lake water level (LWL) and extent (LWE), lake surface water temperature (LSWT), water colour (lake water leaving reflectance - LWLR) with associated Chlorophyll-a (Chl-a) and turbidity, ice cover (LIC) and thickness (LIT). This includes aiming for the longest period of satellite observations suitable for each specific variable, by designing and operating processing chains that ultimately feature in a sustainable data production system.

A key ambition associated with this objective is to establish wide uptake by a varied and fragmented landscape of potential users. This requires significant alignment of current practices for producing the individual Lakes ECV products, cross-variable validation, data harmonisation and, finally, demonstration in the form of use cases. Successfully tackling the challenge of producing a single data set for the Lakes ECV creates an opportunity to move the science community towards wider uptake of Earth Observation (EO) data in limnological studies.

Climate Data Research Package v3.0.0 will include new work to integrate lake ice thickness, lake storage change, Coloured Dissolved Organic Matter (CDOM) and transparency ($K_d$) products. Work on inter-product consistency has continued in preparation of CRDP v3.0.0 while algorithm improvements have been implemented where possible. Coverage of the main hydrological variables (water level and extent) has also further improved.

The CRDP supports different scales of application (e.g., single lake and year, time series, regional and global lake coverage) to meet diverse user needs. This final version of the document does not repeat several local and regional studies which were reported previously in CAR versions v2.0.2.2 and available through the project website. The previous version also includes global studies there were since published in the scientific literature and are not repeated here anymore. Instead, this report will focus on different continental and global scale studies. These reports include:

- Global analysis of lake colour: using LWLR data from 2002 to 2022, changes in water colour across 2024 lakes were assessed. This preliminary analysis, based on the Lakes_cci dataset, reveals notable shifts that may indicate broader ecosystem changes.
- Global Assessment of Water Quality Dynamics: LWLR-derived Chl-a and turbidity data were analysed to assess global changes in phytoplankton abundance across 2024 lakes over a 20-year period, offering insights into shifts in trophic status and particulate matter concentrations. The results reveal a general trend of lakes transitioning from low-to-medium trophic and turbidity levels toward higher Chl-a and turbidity values, indicating a decline in overall water quality.
- Effects of climate extremes in sub-Sahelian African lakes: in most extreme events, clear links emerged between precipitation, temperature, and water quality variables such as turbidity and

Chl-a. These patterns suggest that compound extremes can degrade lake water quality, though the complex interplay of climatic and water quality factors makes it challenging to isolate individual drivers.

This document provides updates on the three new specific use cases, specifically on:

- Heatwave and storm event impacts on lakes: the analysis of lake responses to the 2019 heatwaves in Europe and India highlighted the importance of lake morphology in shaping the timing and intensity of water quality responses to heatwaves. Mean lake depth played a key role in determining Chl-a response patterns, with deeper lakes generally responding more synchronously than shallow ones. In India, turbidity dynamics were primarily driven by precipitation, reflecting the strong influence of monsoon seasonality in the region
- Water quantity in relation to water quality in a changing environment:
    - a case study on Lake Qadisiyah (Iraq) assessed long-term changes in water level and quality under La Niña conditions. Results showed that water level declines were primarily driven by La Niña-induced droughts (as indicated by the SPI). Increases in Chl-a were mainly linked to expanding built-up areas and a reduction in catchment water surface, while water area changes were the main factor influencing turbidity
    - At the global scale, combined analysis of water level and turbidity revealed complex seasonal and interannual dynamics, with 86% of the reservoirs showing a negative relationship between water level and turbidity.
- Climate indicators for the global lakes dataset: the report introduces enhanced features of the Climate Indicators Dashboard, demonstrating its regional applicability. In China, the dashboard reveals an increasing frequency of heatwaves in lakes between 2002 and 2022, with a sharp rise in recent years across all lake size categories. In Greenland, it shows a substantial reduction in lake ice cover, particularly in lakes below 1000 m, where a 30% decline per decade is observed. Similarly, in Sweden, the dashboard indicates a consistent decrease in ice cover duration across all elevations, with the most significant reductions in lowland lakes.

The document also provides updates on the external literature review from 2025, demonstrating how Lakes_cci supports research and applications in the wider scientific community.

# 2 Introduction

## 2.1 Purpose and structure of this document

The purpose of the document is to provide an overview of the value of Lakes_cci products and associated activities in the context of climate science. The document herein presents the findings derived from the activities undertaken within the scope of the project. These activities include CRDP assessment, data exploration and the application of case studies. The analysis concerns CRDP v2.1.0, as CRDP v3.0 will be released later in 2025. The document also includes an update of the review of external studies.

The first part of the document provides a comprehensive overview of the products generated in the Lakes_cci (see Section 3). Section 4 provides an overall data exploration of these products. Section 5 is dedicated to the use of the ECVs at continental and global scales, and Section 6 includes outcomes from Use Cases. An updated evaluation on externally published work is reported in Section 7. The final section (Section 8) presents the key conclusions that have been drawn from the analysis.

# 3 Products of the Lakes_cci project

Lakes_cci projects has developed the latest generation satellite EO products for lakes globally. A set of 2024 inland waterbodies distributed globally have been selected as targets. The data set contained in CRDP v2.1.0 spans 1992 to 2022 for some variables, or shorter periods as satellite assets allow. Indeed, due to the heterogeneity of missions and sensor, it is important to bear in mind that data is not available for all targets over the entire period, nor at the same temporal resolution. The data set is supplied in the same temporal and spatial framework in NetCDF format and makes up the Lakes Essential Climate Variable (ECV) with the following products:

Lake Water Level (LWL) is the measure of the absolute height of the reflecting water surface beneath the satellite with respect to a vertical datum (geoid) and expressed in metres. LWL is a fundamental proxy to understand the balance between water inputs and water loss and their connection with regional and global climate changes.

Lake Water Extent (LWE) refers to the extent (or area) of a lake covered by water, it is a proxy for change in glacial regions (lake expansion) and drought in many arid environments. Water extent can influence the local climate, for example having a cooling effect. This variable can also provide information for ongoing processes in the littoral zone of a lake, crucial for lake catchment-basin interactions and key habitat for many biological communities.

Lake Surface Water Temperature (LSWT) is defined as the temperature of the water at the surface of the water body (surface skin temperature). LSWT is correlated with regional air temperatures and can be a proxy for mixing regimes, driving biogeochemical cycling and seasonality.

Lake ice cover (LIC) refers to the extent (or area) of a lake covered by ice. Timing of freeze-up in autumn and advancing break-up in spring are proxies for gradually changing climate patterns and seasonality.

Lake Ice Thickness (LIT) can be considered a driver of seasonal lake biogeochemistry and early indicator of changing lake thermodynamics.

Lake Water-Leaving Reflectance (LWLR), also referred to as water colour, is the measurement of the quantity of sunlight reaching the remote detector after interaction with the water column. From LWLR, chlorophyll-a (Chl-a) and turbidity have been derived. LWLR represents a direct indicator of biogeochemical processes in the visible part of the water column (e.g., seasonal phytoplankton biomass fluctuations and blooms) and can be used to trace the frequency of extreme events (e.g., peak terrestrial run-off, changing mixing conditions).

Each of the Lakes ECV products has associated uncertainty estimates and quality flags.

Given the diversity of variables and methods used to collect, analyse and provide the data, we recommend reading the following documents prior to using the Lakes_cci dataset.

- Product User Guide (PUG).
- End-to-End ECV Uncertainty Budget (E3UB;).
- Algorithm Theoretical Basis Document (ATBD;).
- Product Specification Document (PSD).

# 4 Data exploration

The data presented in this CAR are based on the CRDP version v2.1.0 for 2024 inland waterbodies of which 84% are lakes and 16% are reservoirs A descriptive table of all locations and the availability per ECV product is provided through the project website (https://climate.esa.int/en/projects/lakes/data). The data set has improved product quality filters and flags and coverage of LWL and LWE compared to the previous releases (v1.0.0 and v2.0.0). The satellite products (Carrea et al., 2023) have the following main characteristics:

- Daily aggregation interval pinned to 12:00:00 UTC.
- Grid format with spatial resolution of 1/120 degrees (near 1 km at the equator).
- Per-lake variables (LWL and LWE) are duplicated into the grid for the area given under the nominal spatial delineation of that lake, derived from its maximum water extent as used for the variables resolved for the whole lakes grid.
- Datum: WGS84.
- Extent: -180 to 180 degrees longitude, -90 to 90 degrees latitude, where positive signs point north and east. The pixel coordinate is the centre of the pixel. This results in 21600 grid rows and 43200 grid columns.
- Spatial coverage: 2024 globally distributed lakes.
- 1 netCDF file per day containing all thematic variables (except Lake Ice Thickness)
- Temporal coverage: from 1992 up to 2022 (LWL/LWE: 1992-2022; LIC2000-2022; LSWT: 1995-2022; LWLR: 2002-2022).

CRDP V2.1.0 is available at the Centre for Environmental Data Analys, CEDA (lakes_cci v2.1.0). Follows some important update compared to the previous release:

- LWL/LWE: increased spatial coverage and better temporal coverage for some lakes using additional data from past missions. Improvement in time series due to geoid correction (after 2020).
- LSWT: reprocessed SLSTR/Sentinel3A/B for CRDP v2.1.0 and found slight degraded performance for SLSTRA in 2021 and 2022; therefore, SLTRA was excluded, and dataset created with SLTRB and MODIS.
- LIC: increased temporal coverage.
- LIT: new product added for demonstration over Great Slave Lake only. This product is provided in three separate files, one per orbit pass number observing the lake.
- LWLR: new quality flags for LWLR including from inter-product consistency checks, and harmonisation of variable naming for wavebands in close proximity but on different sensors.

## 4.1 The Lakes_cci data at a glance

### 4.1.1 Global distribution of ECVs

The global distribution of the lakes included in V2.1.0 is showed in Figure 1. Of the 2024 waterbodies 1700 are classified as lake, 324 as reservoir.

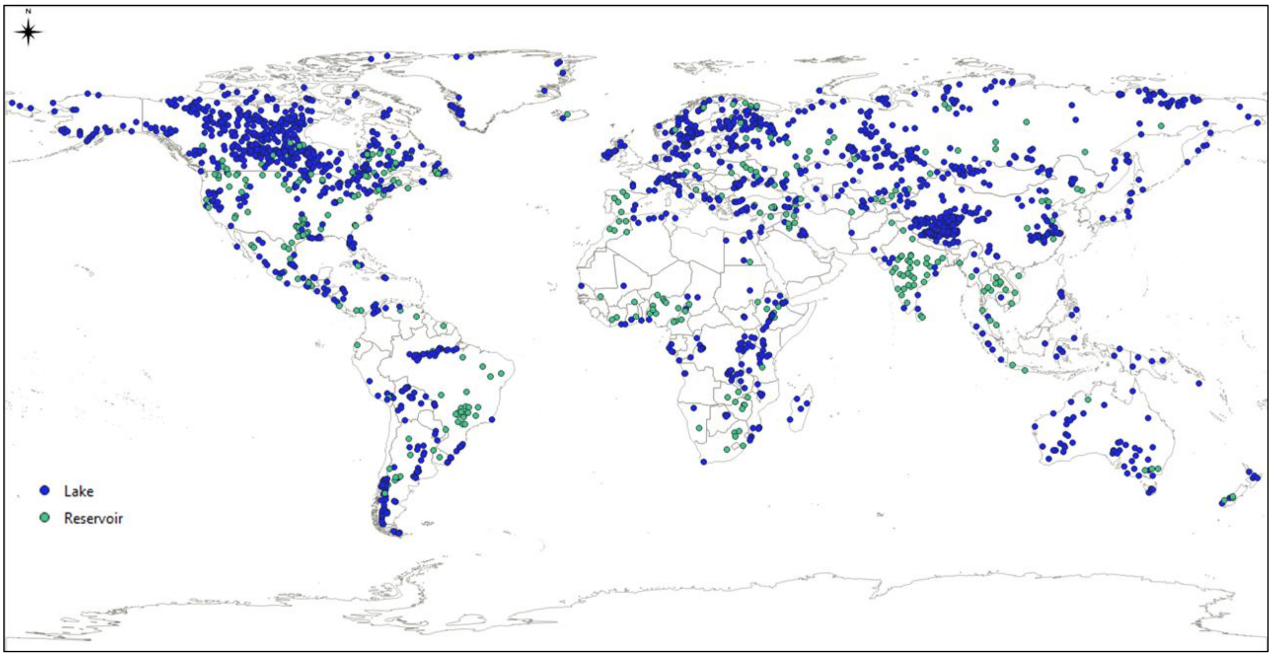


Figure 1. Global distribution of the Lakes_cci dataset (CRDP v2.1.0).

Satellite products for the 2024 lakes extracted from the NetCDF files were used to illustrate the temporal distribution of each thematic variable across the years. Uncertainty layers associated with the ECVs were used to filter the data. The level of acceptable uncertainty is application-specific and for this exploration we used the criteria listed in Table 1.

The following data processing steps were performed:

- Filtering data (water temperature, water level, water extent, Chl-a, turbidity) according to associated uncertainty/quality indicators (Table 1).
- Extraction of mean values based on lake vector definitions.
- Removal of Chl-a and turbidity data when ice cover data is also present to avoid ice interference on water quality data.
- Threshold settings: i) LSWT, values < 200 K and > 374 K; ii) Chl-a, values <0.0001 mg $m^{-3}$ and >300 mg $m^{-3}$; iii) turbidity, values <0.0001 mg $m^{-3}$ and >1000 mg $m^{-3}$.
- Removing extreme outliers (>5 times the inter-quartile range, IQR).
- Conversion to time series.
- Calculating monthly and annual averages.
- Some variables were normalised for allowing comparison (described below).

Table 1. Quality control filters used when extracting data for this assessment

| Thematic variable | Applied approach |
|---|---|
| *Temperature* | Selection limited to LSWT quality level 4 – 5. |
| *Level* | Not filtered. |
| *Extent* | Error is standard value per lake – not filtered. |
| *Chlorophyll-a* | Filtered by an uncertainty of 60%. |
| *Turbidity* | Filtered by an uncertainty of 80%. |

Plots indicating the data distribution over time, calculated per lake, are showed in Figure 2, Figure 3, Figure 4, Figure 5, Figure 6.

For Chl-a, turbidity and LSWT the annual average calculated per lake for CRDP v2.1.0. Data seasonality is not considered in this analysis. The distribution plots are here proposed to examine consistency in data distribution for the different Lakes_cci products and not intended to explain global climatic trends.
Data distribution of LWL for the global dataset is reported with normalised data calculated as annual average divided by time series average.
For LWE, data referred to the number of lakes for which Sentinel-2 derived products (2016-2022) are available at a global scale.

The distribution of Chl-a concentration, presented as the annual average per lake, is showed in Figure 2 for CRDP v2.1.0 (2024 lakes). Some outlier Chl-a values have been removed for visualisation purposes. The previously reported gap period between 2013 and 2015 was due to the end of life of ENVISAT-MERIS sensor and the launch of the new Senintel3-OLCI sensor. The period has now been filled for about 48 lakes with MODIS data. Chlorophyll-a dataset showed a unimodal distribution with most of the concentrations centred around 10 mg $m^{-3;}$ however, for the 2013-2015 period the dataset shows a broader distribution, with concentrations centred around 6 mg $m^{-3}$. No specific direction of change in Chl-a was observed for the global dataset over time.

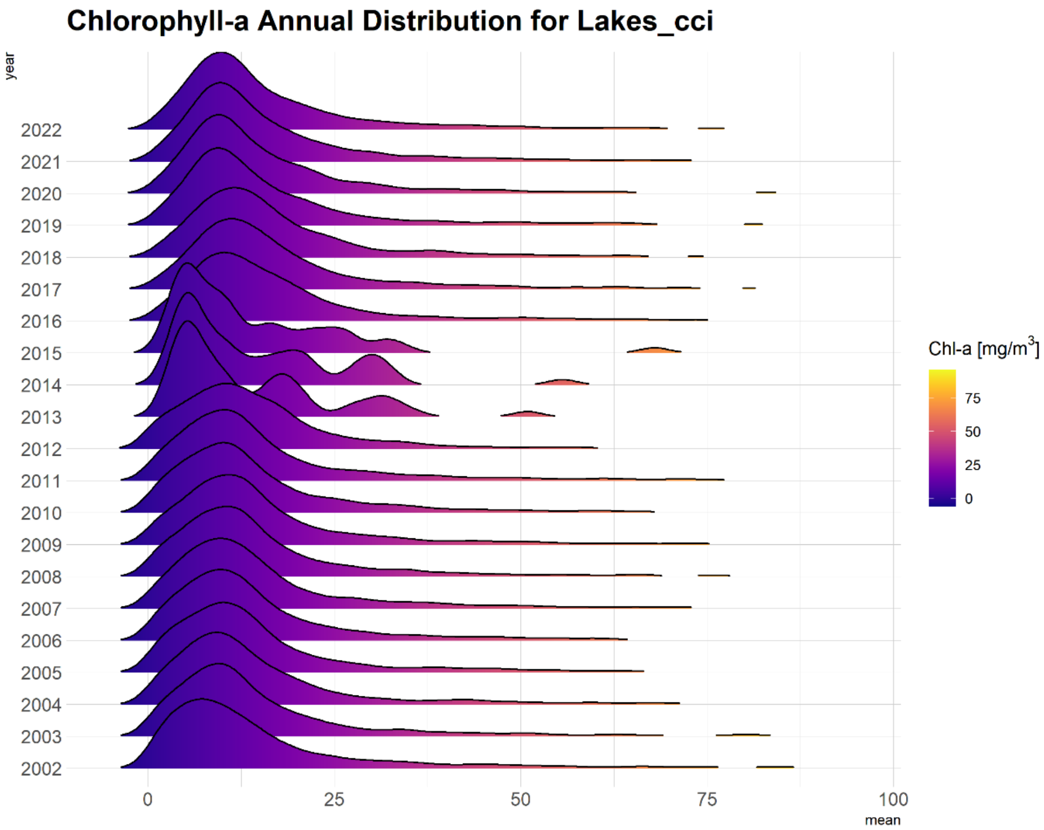


**Figure 2. Distribution of Chl-a concentration, annual average calculated per lake from 2002 to 2022. 48 lakes were used for the period 2013-2015 when MODIS was used to retrieve LWLR.**

Distributions of turbidity (NTU) as derived from the annual average per lake for CRDP v2.1.0 is reported in Figure 3. Some outliers have been removed for clarity. As for Chl-a, the previously reported gap period between 2013 and 2015 has now been filled for about 48 lakes with MODIS data. In the recent datasets turbidity distribution was unimodal with concentration at the beginning of the time series centred around

2 NTU, showing a slight increase over time.  However, for the 2013-2015 period the dataset showed to be distinctly different, with a much narrower distribution and with concentrations centred around 1 NTU.

The distribution of both Chl-a and turbidity for the period 2013–2015 is clearly influenced by the smaller number of lakes covered during this period. Therefore, this should be taken into account when interpreting the results.

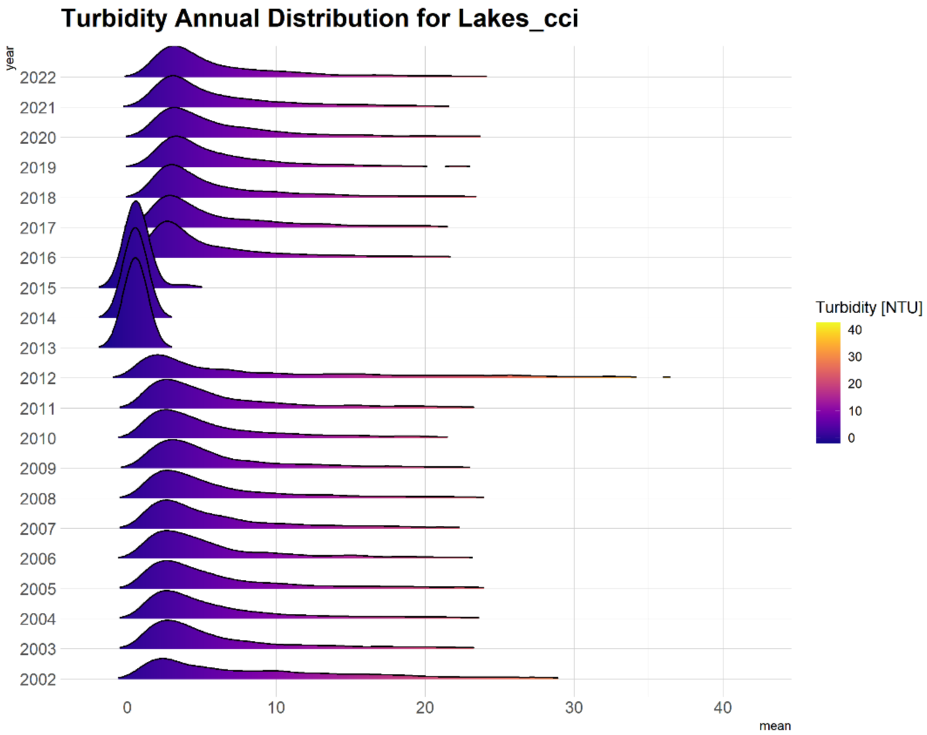


**Figure 3. Distribution of turbidity (NTU), annual average calculated per lake from 2002 to 2022. 48 lakes were used for the period 2013-2015 when MODIS was used to retrieve LWLR.**

Global distributions of lake surface water temperature (LSWT; °C) is showed in Figure 4, as the annual average calculated per lake for CRDP v2.1.0. Note that bimodal distributions are derived from lakes being either close to temperate or equatorial regions. The main peak was centred at about 12°-14°C, depending on the years, while a smaller peak was at ≤ 10°C.

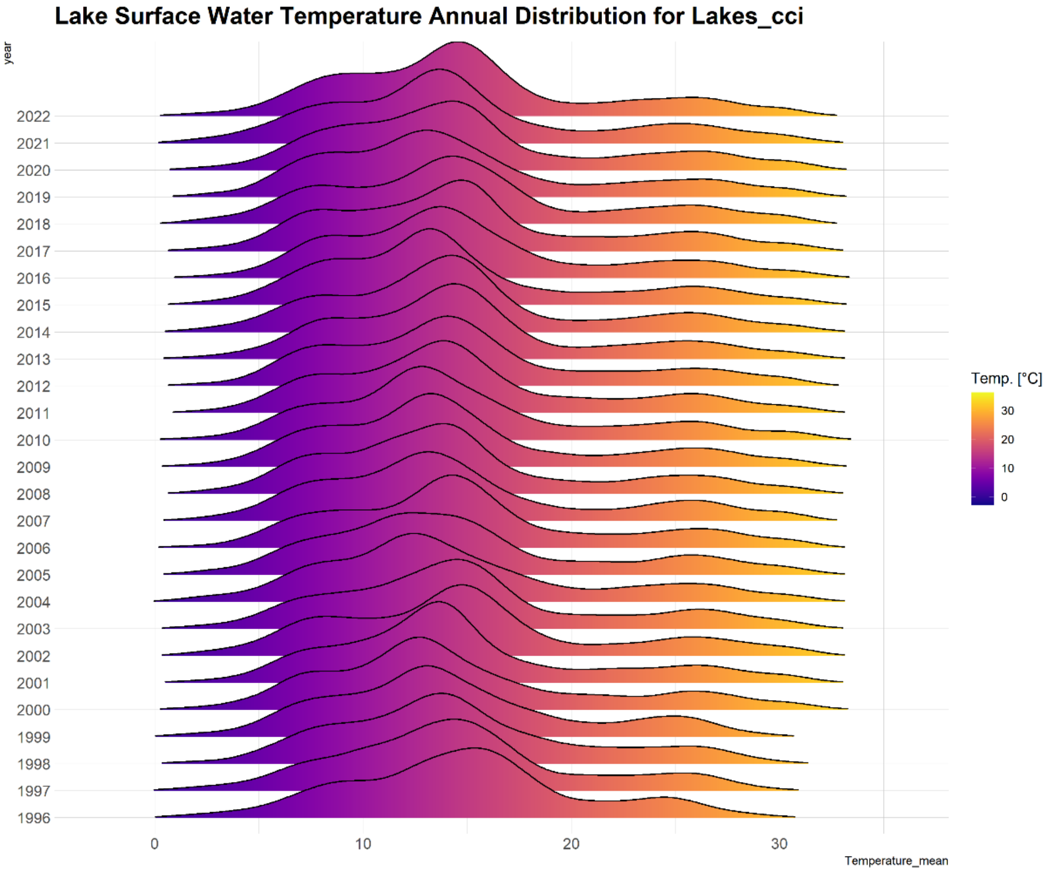


**Figure 4. Distribution of lake surface water temperature (LSWT; °C). Annual averages calculated per lake from 2002 to 2022 (2024 lakes). Note that bimodal distributions are derived from lakes being either closer to temperate or equatorial regions.**

The distribution of normalised LWL and LWE was determined by dividing the per-lake annual average by the time series average for CRDP v2.1.0, as showed in Figure 5 and Figure 6. The lake level distribution is centred around 100% and remains stable over time. It is not currently possible to speculate on the LWE graph.

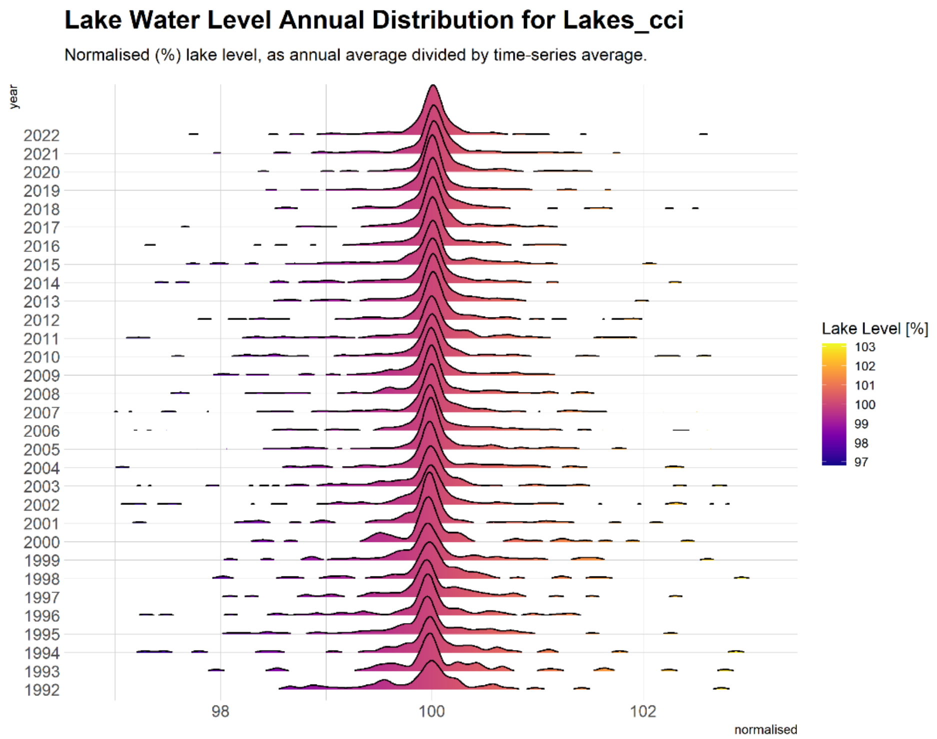


Figure 5. Distribution of normalised (%) lake level, calculated per lake as annual average divided by time series average, for the global dataset. Scaled between 96-104% for clarity.

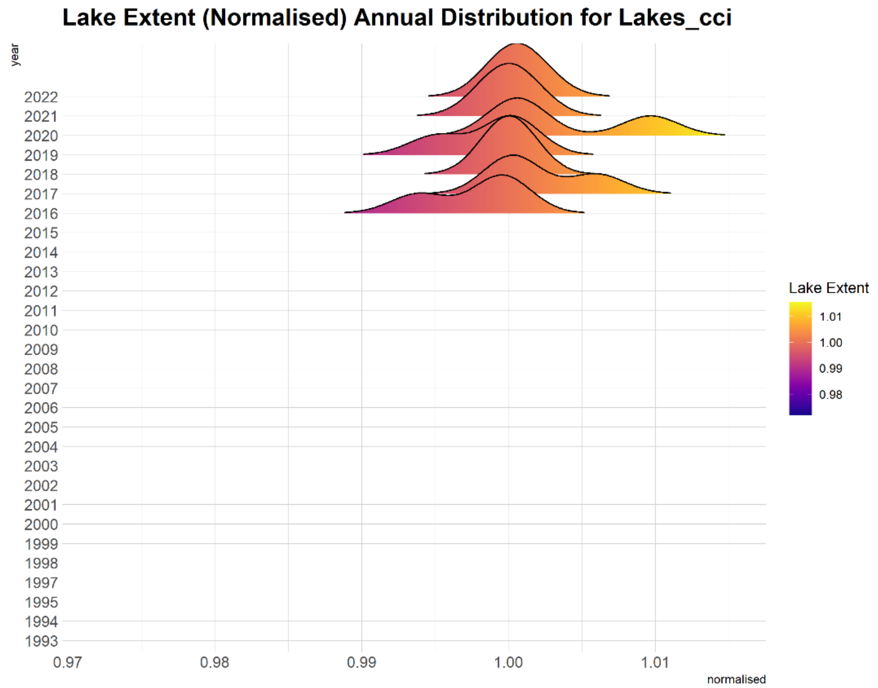


Figure 6. Distribution of normalised (%) lake extension, calculated per lake as annual average divided by time series average, for the global dataset.

## 4.2 ECV products update in v3.0

The following updates are scheduled for v3.0 in Q4 2025:

- LWL*:* increase in spatial coverage (498). Some lakes being processed with LPP algorithm (described in ATBD). Reprocessing of lakes being observed by Sentinel-3A and Sentinel-3B missions with T-IPF products, which improve LWL estimates mainly over small lakes and shorter transects.
- LWE: increase in spatial coverage, and validation of the LWE extraction process from Sentinel-2.
- LSC*:* this new lake product contains the lake storage change.
- LSWT: attempt to increase spatial coverage exploring nighttime LSWT for the largest lakes and a readjustment for the bias between instruments increases alignment between LSWT from different instruments.
- LIC: addition of per-pixel uncertainty for Random Forest classification and a temperature filter to remove/limit influences of turbid water and algae blooms on classification accuracy. New variables are added including lake ice cover extent and lake ice area coverage as well as comparisons to other LIC products.
- LIT**:** time series with LIT product for 13 lakes.
- LWLR: fine-tuned algorithms for MERIS, OLCI and MODIS following an upgrade of the atmospheric correction for LWLR. Chl-a and total suspended matter (TSM; new product replacing turbidity) are fully recalibrated, and new calibrated algorithms are used to add the vertical diffuse attenuation ($K_d$) in three wavebands and aggregated over PAR. Coloured Dissolved Organic Matter (CDOM) absorption at 442 nm is also added for the first time. Uncertainty products for $K_d$ are not separately included, but may be considered to have the same relative uncertainty as the equivalent LWLR wavebands.

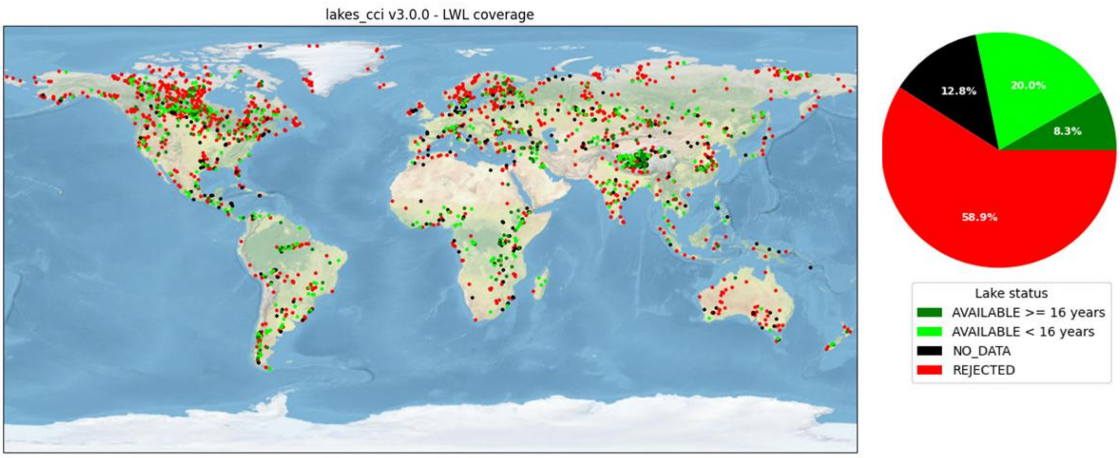


Figure 7. **Overview of the LWL product availability in global coverage and in time series for the target period 1992–2022. Lakes with data available for at least 50% of the target years (dark green dots), lakes with data available for less than 50% of the target years (light green dots), lakes not observed by altimetry satellite missions (black dots) and lakes rejected due to unsatisfactory observation or product quality (red dots).**

# 5 Global scale assessment

## 5.1 Global analysis of lake colour

Although the perceived colour of water is not unequivocally correlated with specific quantitative water quality parameters such as clarity, phytoplankton concentration, suspended particulate matter, and CDOM, it remains a valuable qualitative indicator. The visual appearance of water provides an intuitive representation of water quality, facilitating effective communication and public understanding. Furthermore, as it does not rely on knowledge on optical properties and concentrations of water components, remote sensing methods estimating the colour of water has been widely applied from regional to global scale both in oceans (e.g. Pitarch et al., 2019) and lakes (e.g. Lehmann et al., 2018; Yang et al., 2022; Shen et al., 2025) helping to capture both short- and long-term responses to climate fluctuations.

We used LWLR from 2002 to 2022 to estimate the evolution of water colour in the 2024 lakes. Following Shen et al. (2025), all lakes with an average depth < 2.2m (n = 207) were excluded from the analysis to rule out the interference of bottom reflectance. A total of 1645 lakes were analysed. First, daily observations of Rrs were used to calculate the dominant wavelength ($\lambda_{dom}$) in the chromaticity colour space per lake per day and classified using the following thresholds: blue ($\lambda$ < 495 nm), green (495 nm ≤ $\lambda$ < 560 nm), yellow (560 nm ≤ $\lambda$ < 590 nm), orange (590 nm ≤ $\lambda$ < 640 nm) and red ($\lambda$ ≥ 640 nm). Daily $\lambda_{dom}$ values were aggregated on a monthly level using the median. To identify the dominant colour of the respective month, a threshold of ≥ 60% of observations was used. This means that if in a month e.g. 65% of daily observations were of $\lambda_{dom}$ in the blue range, blue was assigned as the dominant colour. If, within a single year, a lake has less than 6 valid observations, the year was excluded from further analysis (=NA). The median $\lambda_{dom}$ was then calculated per year per lake and aggregated into 5-year periods, with a gap from 2012-2016. This resulted in three 5-year periods (2002-2006, 2007-2012, 2016-2020) and one period spanning the last years available in version 2.1.0, 2021-2022 (Figure 8).

At the beginning of the timeseries, we can visually observe (Figure 8) a cluster of blue lakes in Patagonia that remained present until 2021–2022. The same occurred for blue lakes located at higher latitudes in eastern North America and around the Himalayas. By contrast, the number of blue lakes in northern Europe and Canada decreased between 2002 and 2022. Yellow-dominated lakes are distributed globally in the time series, with clusters in Australia, Canada and Central Asia between latitudes 40° and 60° N, and Central and South America. Green lakes are mostly found in North America and Europe. In Africa, green and yellow lakes are both well represented.

Blue lakes represented 5-6% in the four periods examined, while green and yellow lakes ranged from 40% to 54% and 30% to 37%, respectively (Figure 9). Orange and red dominant wavelengths were uncommon and therefore negligible in the aggregation. NA (not applicable) was assigned when an insufficient number of monthly aggregated observations were available (ranging from 4% to 24%). The NA percentage was higher in the first two periods and lower in the more recent years, meaning that a higher number of valid observations are available (Figure 9). Examining the changes in colour class over 5-year periods, we can observe an increase of around 15% in green lakes and around 5-7% in yellow lakes from the first decade (2002-2012) to the final two analysed periods (2016-2022) (Figure 9).

To analyse the changes in colour class experienced by global lakes, we considered the beginning (2002-2006) and end of the time series (2021-2022), excluding lakes with insufficient data (NA) in either of those periods. This represents 1199 lakes, 17% (n=199) of which changed colour class. 43% of these changing lakes passed to a class with a lower dominant wavelength. All of the blue lakes (n=24) moved to a class with a higher dominant wavelength (green). Meanwhile, the green lakes (n=111) moved to classes with both lower and higher dominant wavelengths: 21% became blue, while 79% became yellow. Almost all the yellow lakes (n=64) that changed class moved to a lower dominant wavelength.

Our results are partially consistent with those of Shen et al. (2025), who examined long-term colour trends in 67,579 lakes worldwide between 1984 and 2021 from Landsat 5, 7 and 8. They found that blue lakes (< 495 nm) were mainly located in high-latitude and high-elevation regions, green lakes (495–560 nm) were mostly found in densely populated mid-latitudes, and red/yellow lakes (≥ 560 nm) were predominantly present in the Southern Hemisphere. The researchers found that most lakes showed a shift towards shorter wavelengths over time, particularly in warm temperate and boreal zones. Previous work by Yang et al. (2022a) used 5.14 million satellite-derived colour records from 2013 to 2020 to identify the modal water colour of 85,360 lakes worldwide, based on dominant wavelength values from Landsat 8. They found that lake colours span the visible spectrum and exhibit a clear bimodal distribution: 31% were blue, while 69% were non-blue (ranging from green to brown). They suggested that the modal colour is influenced by climate and lake morphology. Blue lakes are typically found in regions with cooler summers, winter ice cover, and higher precipitation. They also speculated that under climate projections of a 3°C rise in summer air temperature, 14% of blue lakes could change to a non-blue colour, indicating significant ecological change.

This preliminary analysis of water colour derived by the Lakes_cci reveals significant shifts that may signal broader ecosystem transformations. As future lake colour trends are expected to evolve further, these findings provide a first insights for understanding the water conditions while a further classification in terms of optical water types (e.g. Spyrakos et al., 2018) might complete the picture in terms of distinguish turbid lakes, high productive waters, humic rich lakes etc. and informing effectively the stakeholders (e.g. conservation policies).

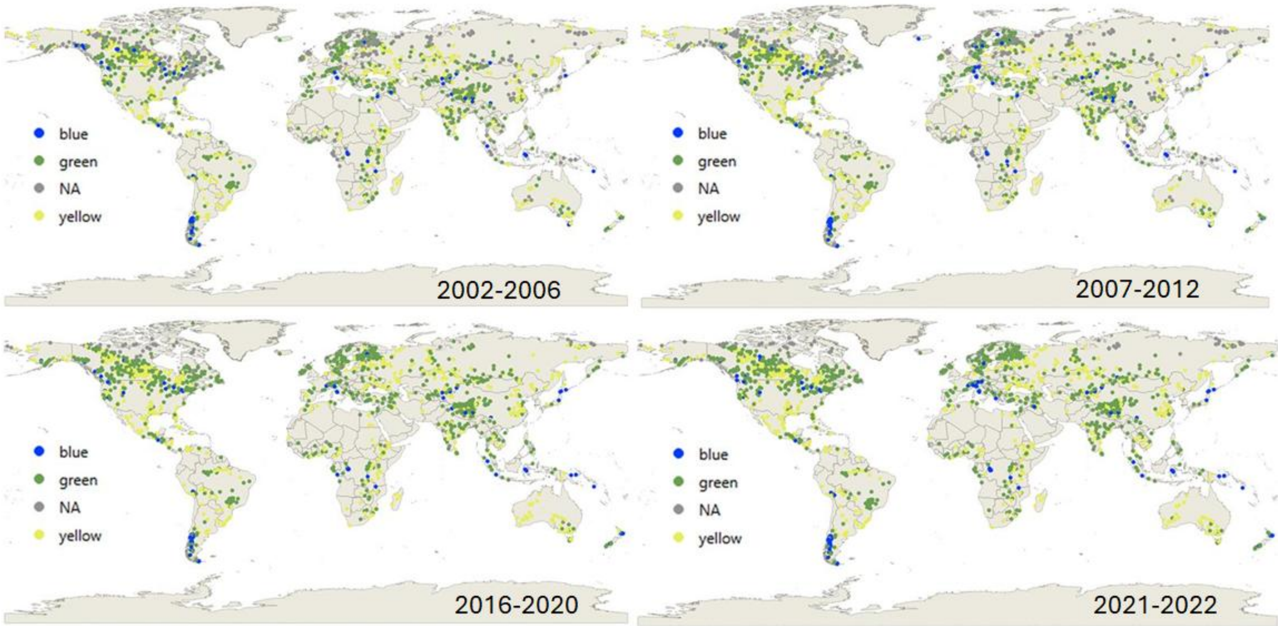


Figure 8. Median values of the dominant wavelength for the four periods from 2002 to 2022. The colours represent the following wavelength ranges: blue (λ < 495 nm), green (495 nm ≤ λ < 560 nm), yellow (560 nm ≤ λ < 590 nm), orange (590 nm ≤ λ < 640 nm) and red (λ ≥ 640 nm). NA: lake excluded from further analysis as it had less than six valid observations in a single year.

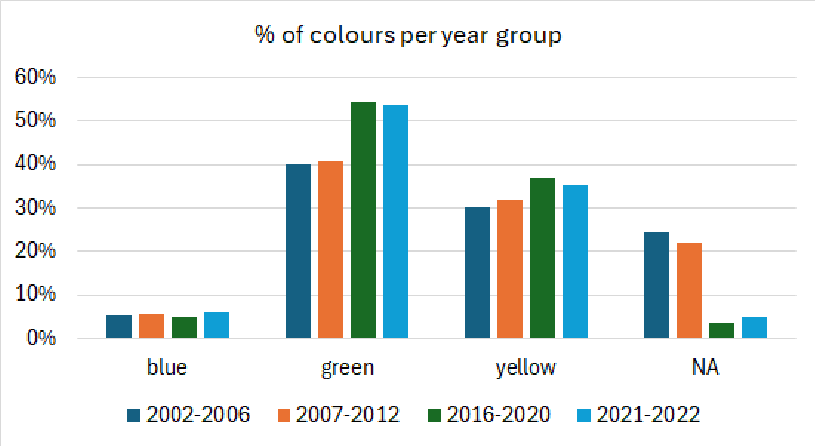


Figure 9. Percentage of lakes in each of the four colour groups of the dominant wavelength in the four investigated periods. The colours represent the following wavelength ranges: blue ($\lambda$ < 495 nm), green (495 nm ≤ $\lambda$ < 560 nm), yellow (560 nm ≤ $\lambda$ < 590 nm), orange (590 nm ≤ $\lambda$ < 640 nm) and red ($\lambda$ ≥ 640 nm). NA: lake excluded from further analysis as it had less than six valid observations in a single year.

## 5.2 Global Assessment of Water Quality Dynamics

Water quality plays a crucial role in aquatic ecosystems and typically describes the chemical, physical, and biological properties of water that determine its suitability for various uses. Monitoring water quality is essential for conserving water resources, preserving ecological integrity, and ensuring human health and safety. It is well known that remote sensing provides technical support for lake water quality monitoring and can be used to monitor many indicators and parameters, including chlorophyll-a and turbidity (e.g., Yang et al., 2022b; Giardino et al., 2019; Dörnhöfer & Oppelt, 2016; Palmer et al., 2015). Therefore, a logical next step after analysing water colour variability is to explore how underlying water quality parameters change over time.

We used LWLR-derived products Chl-a and turbidity to investigate global changes in phytoplankton abundance across lakes (n=2024) over a 20-year period, providing an overview of changes in trophic status and particulate matter concentration, which is related to water transparency. We calculated the mean annual values of Chl-a and turbidity for each lake from daily observations. We then aggregated it as a median value across 5-year periods, with a gap from 2012-2016. This resulted in three 5-year periods (2002-2006, 2007-2012, 2016-2020) and one period spanning the last years available in version 2.1, 2021-2022. The maps showing these results are showed in Figure 10 for Chl-a and in Figure 12 for turbidity.

We observe a clear shift in trophic status for several lake regions over time. In Canada, a cluster of oligotrophic lakes (2002–2006) transitioned to higher trophic classes by the later period (2016–ongoing). In Central Asia, the number of lakes in the oligotrophic "blue" class (<5 mg $m^{-3}$) declined, with many shifting toward mesotrophic conditions. In Patagonia, a persistent cluster of oligotrophic lakes remains, consistent with observed water colour data (cf. Figure 8). In Northern Europe, an increasing number of lakes became eutrophic over the course of the time series. Hypertrophic lakes are primarily found in North America, along Africa's Rift Valley, and in northern regions of the Asian continent. Lakes in other areas, such as Africa and Australia, exhibit a wide range of trophic conditions—from oligotrophic to hypertrophic.

A preliminary overview revealed that oligotrophic lakes accounted for between 8% and 16% of all lakes across the four periods analysed, mesotrophic lakes for approximately 36–39%, eutrophic lakes for 31–39%, and hypertrophic lakes for about 14–17% (Figure 11). Lakes with unavailable classification accounted for approximately 1–2% of the total. We observed a decrease in oligotrophic lakes from 16% in the initial period (2002–2006) to 9% in the final two-year period analysed.

From the beginning of the time series (2002–2006) to its end (2021–2022), Chl-a data were available for 1,991 lakes in both periods. Among these, 35% experienced a change in trophic status class. Of the 709 lakes that changed class, 28% shifted to an adjacent class with lower Chl-a values. Conversely, 66% moved to a higher trophic status class, and 5% worsened by two or more classes. Oligotrophic lakes (n=177) mainly moved to mesotrophic class (91% of lakes), while mesotrophic lakes (n=255) mainly increased of one class (83%), but also shifted to lower classes (8%). Eutrophic lakes (n=219) moved mainly to higher trophic status classes (43% of lakes), but also to a lower Chl-a class (56%). Of 58 hypertrophic lakes, 91% moved to eutrophic class.

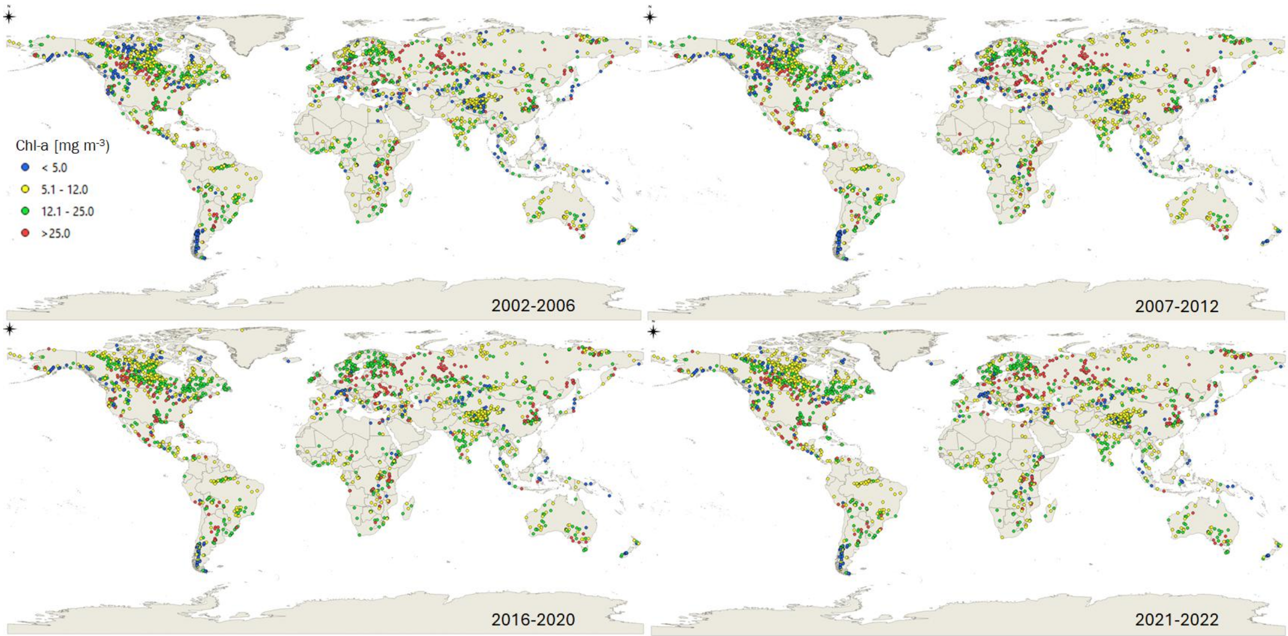


**Figure 10. Median Chl-a concentration in the years 2002–2006, 2007–2012, 2016–2020 and 2021–2022.; 5-12, The colours represent the following trophic classes: oligotrophic <5 mg m⁻³, mesotrophic 5-12 mg m⁻³, eutrophic 12-25 mg m⁻³, and hypertrophic >25 mg m⁻³.**

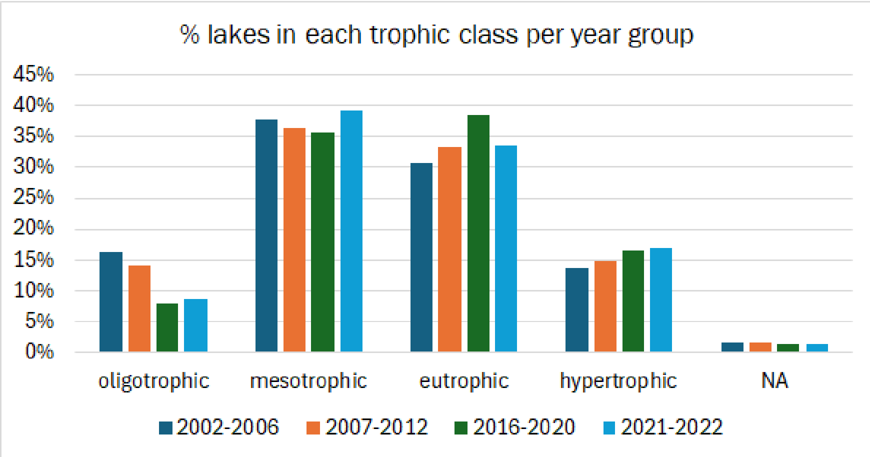


**Figure 11. Percentage of lakes in each of the four trophic status classes (oligotrophic <5 mg m⁻³, mesotrophic 5-12 mg m⁻³, eutrophic 12-25 mg m⁻³, and hypertrophic >25 mg m⁻³); not applicable for a low number of observations (NA).**

As shown in Figure 12, until 2012, lakes in Canada predominantly exhibited very low median turbidity concentrations. However, in the two most recent periods, these lakes shifted to a slightly higher turbidity class. Clusters of lakes with high or very high turbidity levels (represented by orange and red dots) are found in the Himalayan region, parts of Africa, and Australia. Similar to patterns observed in water colour and trophic status, lakes in the Patagonian region are dominated by the two lowest turbidity classes.

A preliminary overview revealed that lakes with turbidity ≤2 NTU accounted for between 6% and 14% of all lakes across the four periods analysed; those with turbidity between 2 and 5 NTU for approximately 41–48%; those with turbidity between 5 and 10 NTU for about 22–24%; those between 10 and 20 NTU for about 8–10%; and lakes with the highest turbidity (>20 NTU) for about 8–10% (Figure 13). Approximately 1–2% of the total lakes could not be classified. We observed a decrease of 8% in the lowest turbidity class (≤2 NTU) between the first and the last period analysed, and a slight increase in the medium turbidity classes (2–5 and 5–10 NTU) of approximately 4% and 2%, respectively.

From the beginning of the time series (2002–2006) to its end (2021–2022), turbidity data were available for 1,991 lakes in both periods. Among these, 45% experienced a change in turbidity class. Of the 897 lakes that changed class, 26% shifted to an adjacent class with lower turbidity values, and 6% improved by two or more classes. Conversely, 60% moved to a higher turbidity class, and 8% worsened by two or more classes. Lakes in the lowest turbidity classes at the beginning of the time series (≤2 NTU, n = 200; 2–5 NTU, n = 268) predominantly shifted to an adjacent class with higher turbidity values (94% and 72%, respectively). Lakes in the 5–10 NTU class (n = 244) showed a more balanced pattern, with 41% moving to a higher class and 47% to a lower one. A similar trend was observed for lakes in the 10–20 NTU class (n = 142), with 37% shifting to a higher class and 41% to a lower one.

Water quality dynamics showed a general shift of lakes at low-medium trophic status and turbidity classes versus higher Chl-a and turbidity concentration. These results are in line with other literature studies, such as Caroni et al. (2025) that investigated water quality parameter trend for shallow lakes.

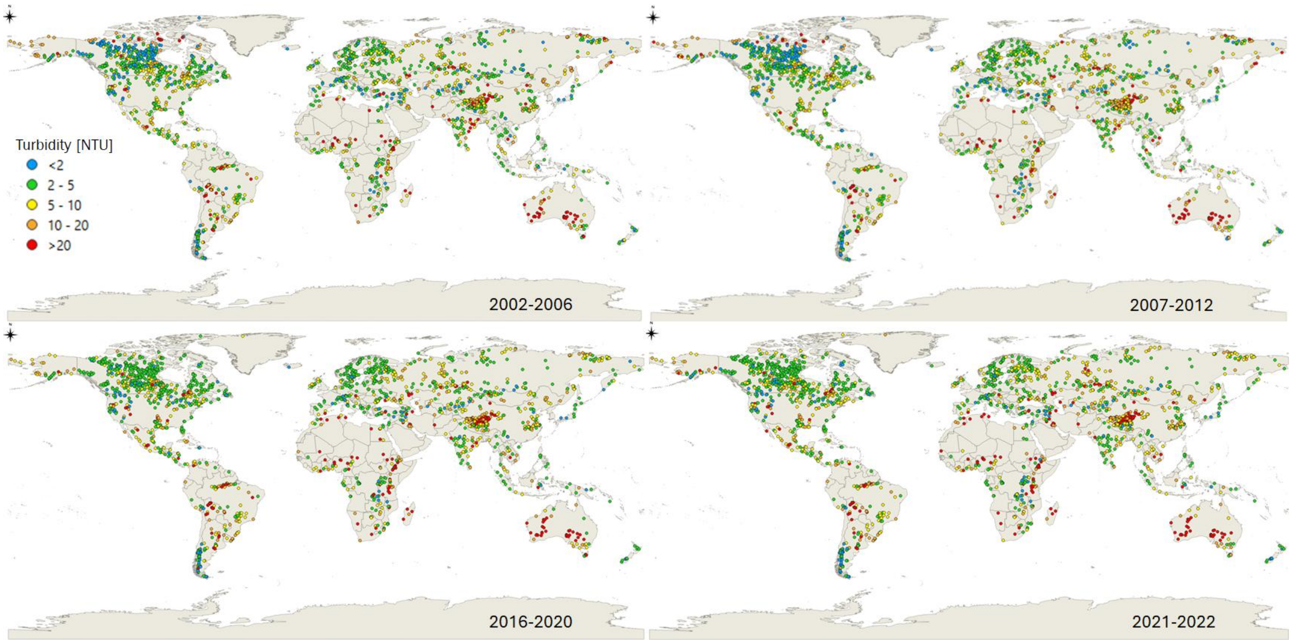


Figure 12. Median turbidity in the years 2002–2006, 2007–2012, 2016–2020 and 2021–2022.

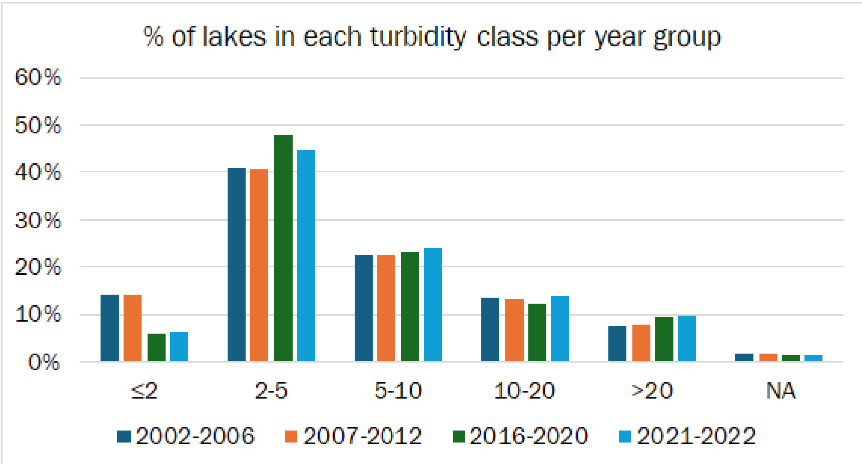


Figure 13. Percentage of lakes in each of the five turbidity classes (NTU: <2, 2-5, 5-10, 10-20, >20) in the four investigated periods; not applicable for a low number of observations (NA).

## 5.3 Effects of climate extremes in sub-Sahelian African lakes

Africa is highly vulnerable to climate change despite its minimal contribution to global emissions, yet this is not reflected in the level of research. The study of lakes on the African continent is limited and concentrated in the African Great Lakes (e.g., Plisnier et al., 2022; Shen et al., 2022). Additionally, there is a significant lack of meteorological and climatic data, as existing systems to monitor and manage extreme events are underdeveloped, resulting in insufficient data availability (Codjoe & Atiglo, 2020). Africa faces both droughts and floods, increasingly intensified by shifting rainfall patterns and rising temperatures. Droughts reduce soil permeability, heightening flood risk when rain returns. The erratic nature of precipitation threatens livelihoods, particularly in agriculture, which depends heavily on rainfall. This also leads to greater pressure on inland water sources, often overused for irrigation during dry periods. Extreme events (EEs), by definition, are those that in the distribution occur within the first or last decile, according to the IPCC (2014). However, these thresholds should be locally adapted, as regional climate variations can significantly alter their relevance (Jeppesen et al., 2021). In this context, the main objective of this study is to examine specific extreme weather events and their effects on water quality variables in a subset of African lakes, using satellite-derived data from the Lakes_cci dataset. Specifically, the study aims to: (i) analyse time series and patterns of meteo-climatic and water quality variables for the selected lakes; and (ii) identify and assess compound extreme events involving these variables during the 2016–2020 period.

### 5.3.1 Methodology

**Lake selection and data sources**

From the 133 lakes in the Lakes_cci dataset located in the Sub-Sahelian region, a subset was selected to represent a gradient of key characteristics: trophic state, mean depth, origin (natural or artificial), and regional distribution. A visual summary of the selection process, including applied thresholds, is provided in Figure 40 (Appendix-1).

The selection began by grouping lakes according to their trophic state, based on the average Chl-a concentrations (2016–2020) from the Lakes_cci dataset, following the OECD classification (Vollenweider & Kerekes, 1982). Lakes located less than 10 km from the shoreline (12 lakes) and those with a mean depth below one meter (6 lakes) were excluded. Only lakes with a surface area larger than 1,000 km² were retained. Further filtering involved analyzing Land Use/Land Cover (LULC) data from the CCI dataset. LULC changes were calculated using pixel differences within a 0.1-degree buffer around each lake, expressed as time series and spatial maps. Only lakes showing notable LULC changes—such as increased agriculture or urbanization, and reduced forest or natural ecosystems—between 2016 and 2020 were considered. The final selection included Lake Kyoga, Lake Volta, Lake Naivasha, Lake Turkana, Lake Kariba, and Lake Tanganyika (). Key features of these lakes are summarized in Table 2.

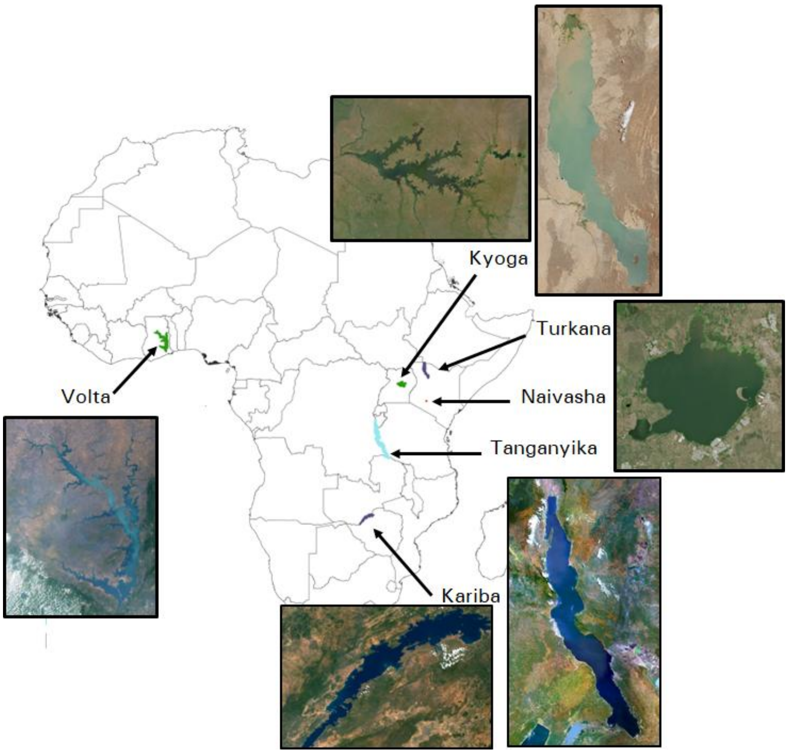


Figure 14. Map showing the six Sub-Sahelian lakes included in the study subset.

Table 2. Main characteristic of the subset of lakes selected for the study.

| Name (ID) | Nat./Art. | Lake area | Trophic Status | Avg. Depth | Secchi Depth |
|---|---|---|---|---|---|
| Tanganyika (7) | Natural | 32759 $km^2$ | Ultra-Oligotrophic | 577 m | 6.1 - 15.5 m |
| Kyoga (100000013) | Natural | 2788 $km^2$ | Eutrophic | 3.0 m | 0.8 – 1.7 m |
| Naivasha (1659) | Natural | 128 $km^2$ | Hypertrophic | 13.6 m | 0.6 – 0.7 m |
| Turkana (22) | Natural | 7473 $km^2$ | Mesotrophic | 31.8 m | 1.0 – 4.8 m |
| Volta (24) | Artificial | 6045 $km^2$ | Eutrophic | 24.5 m | 0.1 – 1.8 m |
| Kariba (35) | Artificial | 5276 $km^2$ | Mesotrophic | 35.1 m | 1.0 – 8.0 m |

The dataset used in this study comprises morphological, meteorological-climatic, biophysical variables, and land cover classification data, with details on variables, sources, and temporal resolution provided in Table 3. The analysis of water quality time series focuses on the period 2016–2020, due to a data gap between 2012 and 2015.

Table 3. Description of the source and resolution of the datasets used in this study.

| Variable | Product | Source | Time step | References |
|---|---|---|---|---|
| *Morphological:*<br>– shore length<br>– lake area<br>– lake volume<br>– lake mean depth<br>– lake elevation<br>– water residence time<br>– discharge average | HydroLAKES (v1.0) | CanVec; SRTM; SWBD; MODIS MOD44W water mask; US National Hydrography Dataset; ECRINS; GLWD; GRanD[1] | Temporal snapshot | Messager et al., 2016 |
| *Morphological:*<br>– lake bathymetry raster | GLOBathy (GLObal Bathymetric dataset) | Global, 1 arcsecond (30 m) | Temporal snapshot | Khazaei et al., 2022 |
| *Land cover classification* - LULC classes | CCI Landcover dataset | MERIS (2002-2012), AVHRR and PROBA-V (2015) - 300 m | 2002 – 2015, expanded by Digital Earth Africa until 2019 | ESA, 2017; Digital Earth Africa, 2022 |
| *Meteo-climatic*:<br>– 2m air temperature (t2m)<br>– surface pressure (sp)<br>– mean surface downward long-wave radiation flux (msdwlwrf)<br>– mean surface downward short-wave radiation flux (msdwswrf)<br>– total precipitation (tp) | ERA5 | Modelled data 31 km | Hourly data on single levels from 1940 to present – Period 1995-2020 and 2016-2020 | Hersbach et al., 2020; Copernicus Climate Change Service, 2023 |
| *Meteo-climatic*:<br>– Rainfall Estimate (RfE) | TAMSAT (Tropical Applications of Meteorology using SATellite data and | Modelled data 4 km | Daily - Period 1995-2020 and 2016-2020 | Tarnavsky et al., 2014 |

[1] Canadian hydrographic dataset (CanVec); Shuttle Radar Topographic Mission (SRTM) Water Body Data (SWBD); MODIS MOD44W water mask; US National Hydrography Dataset; European Catchments and Rivers Network System (ECRINS); Global Lakes and Wetlands Database (GLWD); Global Reservoir and Dam Database (GRanD).

| | | | | |
|---|---|---|---|---|
| | ground-based observations) (v3.1) | | | |
| *Water quality:*<br>– Chlorophyll-a<br>– Turbidity | Lake Water Leaving Reflectance (LWLR) - Lakes_cci v2.0.2 | MERIS (2003–2011) OLCI (2016–2020) 300 m–1 km | Daily - Period 2016-2020 | Carrea et al., 2023 |
| – Lake surface water temperature (LSWT) | Lake surface water temperature (LSWT) - Lakes_cci v2.0.2 | AATSR, AVHRR, SLSTR, and MODIS/Terra–1 km | Daily - Period 2016-2020 | Carrea et al., 2023 |

**Time series, patterns and extreme events**

The analyses of time series and pattern of weather and water quality variables were performed on a brief temporal scale, but the same some patterns could be observed. First, the observations were conducted at a yearly scale to get an overview of temporal patterns for each lake. Then a more in-depth analysis on daily time series have been performed to investigate the presence of extreme events.

To identify EEs, time series data were analysed across three temporal scales - yearly, monthly, and daily. The process began with a visual inspection of annual means, followed by the selection of values significantly above or below these averages. To identify their extreme character, the chosen approach was to calculate the standard deviation and the zeta score ($Z$-score) (Camuffo et al., 2020). Assuming a normal distribution, an observation with a $Z$-score of 1.3 lies above the 90$^{th}$ percentile and therefore can be considered as an extreme event following IPCC. In case of non-normal distributions, the thresholds for extreme events based on the $Z$-score were amended. In addition, the seasonal $Z$-score was calculated, equally to the general $Z$-score, but after grouping the data by month into the lakes' respective seasons. $Z$-scores for each date were plotted including indicators of the 68-95-99 rule. Only those events with a $Z \geq |2|$ and seasonal $Z$-score $\geq |2|$ were considered. In this study, EEs encompass not only extreme weather conditions but also instances where water quality parameters fall within the 10th or 90th percentile of their distribution. Events were analysed both individually and as compound extremes - defined as simultaneous extremes in multiple variables at the same location and time. Following the approach of Woolway et al. (2021), compound events were identified when an extreme in a meteorological variable (e.g., air temperature or precipitation) or LSWT coincided with an extreme in a water quality parameter.

## 5.3.2 Results

This paragraph presents examples of the results obtained for each lake, as well as a summary of the results for all six lakes. More comprehensive details and results can be found in Greife (2023) master's degree thesis and GitHub repository (https://github.com/jgreife/MasterThesis).

**Time series and patterns**

*Lake Kariba for the period 2016-2020*

The timeseries and pattern of precipitation, air temperature, LSWT, Chl-a and turbidity for Lake Kariba for the period from 2016 to 2020 is reported in Figure 15. Lake Kariba typically experiences a single wet season from October/November to April, with peak rainfall occurring mid-season. This pattern remained consistent across years, except in 2018/2019, when rainfall was unusually concentrated in April following a dry spell from February to March. Turbidity showed a clear seasonal pattern aligned with the wet season. However, during 2016/2017, its increase and decrease were more gradual compared to other years. A general decline in turbidity was also observed during the 2017/2018 and 2018/2019 wet seasons, likely linked to reduced cumulative precipitation. These trends are consistent with findings reported by Winton et al. (2021). Chl-a peaks generally lagged behind air temperature maxima. Until 2018, air temperatures rose until November and declined through August. In 2019, however, a secondary temperature rise occurred in February, followed by an unusually high peak in November and elevated values in March and April. These anomalies were mirrored by corresponding increases in Chl-a concentrations. Despite these fluctuations, a gradual decline in average Chl-a levels was observed over the study period. The pattern for LSWT matched that of air temperature.

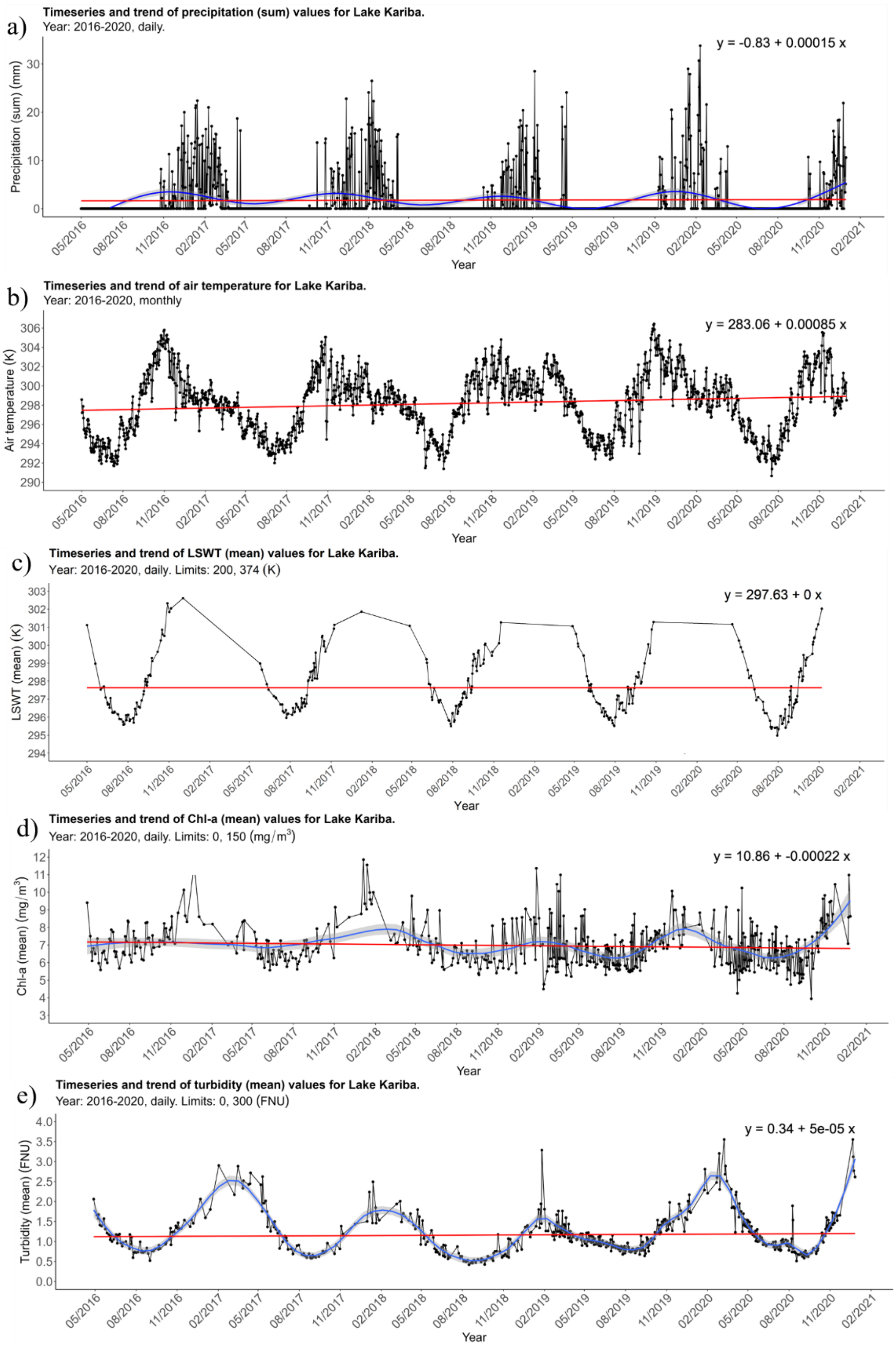

Figure 15. Meteo-climatic and water quality variables in the period of 2016-2020 for Lake Kariba. For each variable a linear regression (red line) was fitted with displayed equations. A smoothed lowess line (blue line) facilitates the patterns in the plots except air and LSWT. a) Timeseries of total precipitation; p-value: > 0.05. b) Timeseries of air temperature; p-value: < 0.001. c) Timeseries of LSWT; p-value: > 0.05. d) Timeseries of chl-a ; p-value: < 0.05. e) Timeseries of turbidity; p-value: > 0.05.

*Patterns in meteo-climatic and water quality variables in all lakes*

Long-term time series (1995–2020) were used for air temperature and precipitation, while water quality variables (LSWT, Chl-a, turbidity) were analyzed from 2016–2020. For consistency, meteo-climatic results were also focused on the 2016–2020 period (Table 4). In the following a summary of trend for each variable is reported.

- Precipitation: Most lakes showed increasing annual precipitation, except Lakes Volta and Kariba, which exhibited declines—particularly for Volta due to low rainfall from 2011–2016. In 2016–2020, only Volta continued to decline. The highest rainfall occurred at Lake Kyoga in 2019; the lowest at Lake Turkana in 2016.
- Air Temperature: All lakes experienced long-term warming since 1995, with the most pronounced rise at Lake Naivasha and the most stable trend at Lake Turkana. From 2016–2020, temperatures remained stable, except for a slight decline at Lake Kyoga.
- LSWT: Slight decreases were observed at Lakes Volta, Kyoga, and Kariba; slight increases at Naivasha and Turkana; and stability at Tanganyika. On a monthly scale, LSWT slightly increased across all lakes.
- Chl-a: Tanganyika, Turkana, and Kariba remained stable; Volta showed a significant decrease ($p < 0.05$); Kyoga and Naivasha increased, though Naivasha's trend may be influenced by peaks in 2017–2018.
- Turbidity: Most lakes showed fluctuations, except for Tanganyika, which remained stable. Turkana showed minimal variation. Increases were noted for Naivasha and Kariba, especially from 2019–2020, while Kyoga and Volta exhibited decreasing trends.

Table 4. Overview of patterns (yearly aggregation) for the meteo-climatic and water quality variables in the period 2016-2020.

| Lake | Precipitation | Air temperature | LSWT | Chl-a | Turbidity |
|---|---|---|---|---|---|
| Volta | ↓ | - | ↓ | ↓ | ↓ |
| Turkana | ↑ | - | ↑ | - | - |
| Kyoga | ↑ | ↓ | ↓ | ↑ | ↓ |
| Naivasha | ↑ | - | ↑ | ↑ | ↑ |
| Tanganyika | ↑ | - | - | - | - |
| Kariba | - | - | ↓ | - | ↑ |

## Extreme events

For the six lakes investigated a series of EEs were identified from the analysis of lake quality variables between 2016 and 2020 (Table 5). However, not all of them were compound EEs.

For this analysis we also used monthly anomalies in LSWT calculated by Brockmann Consult (https://lakescci.climate-indicators.brockmann-consult.de/) for the Lakes_cci indicator and investigated per lake. Overall, the frequency - and in some cases the intensity - of LSWT anomalies increased between 2016 and 2020 across the lakes studied. This trend aligns with global findings reported in the literature. Within this period, each lake experienced approximately 3 to 5 extreme events. For instance, intense rainfall coincided with Chl-a peaks in eutrophic lakes such as Volta and Kyoga, while similar rainfall extremes were associated with turbidity spikes in lakes like Turkana and Naivasha. In lower-trophic lakes such as Tanganyika and Kariba, positive LSWT anomalies were linked to simultaneous increases in both Chl-a and turbidity. Furthermore, Chl-a and turbidity maps were analysed to better support the spatial interpretation of the lake response at extreme weather events.

**Table 5. Extreme events for the six lakes in the period 2016-2020. Chl= Chlorophyll-a, Tu= Turbidity, TP= total precipitation, LSWT=lake surface water temperature.**

| | 2016 | | | | 2017 | | | | 2018 | | | | 2019 | | | | 2020 | | | |
|---|---|---|---|---|---|---|---|---|---|---|---|---|---|---|---|---|---|---|---|---|
| | Chl | Tu | TP | LSWT | Chl | Tu | TP | LSWT | Chl | Tu | TP | LSWT | Chl | Tu | TP | LSWT | Chl | Tu | TP | LSWT |
| Kyoga | | | | | | x | | | | | | | x | | x | | x | x | | |
| Naivasha | | | | | x | | x | x | | | | | x | | x | x | | x | x | x |
| Turkana | | | | | | | | | | | | | x | | | | x | x | x | x |
| Volta | x | | x | | | | | | x | x | x | | | | | | | | | |
| Kariba | | | | | | | | | | | x | | x | x | | x | x | x | x | |
| Tanganyika | | | | | | | | | x | x | | x | x | x | x | | | | | |

As an example, three EEs were identified for Lake Tanganyika, two of which were compound. The selected event, on 15/09/2018, featured a slight positive LSWT anomaly (0.1 K), with concurrent peaks in turbidity (1.1 FNU) and chlorophyll-a (3 mg $m^{-3}$) (Figure 16). This event occurred around the transition from the dry to short wet season in the lake's north, where data was available. Chlorophyll-a concentrations reached up to 10.4 mg $m^{-3}$, with the highest values (>7 mg $m^{-3}$) in the northern and eastern areas, decreasing southward. Central areas showed lower concentrations (<3 mg $m^{-3}$), though streaks of elevated values (5–9 mg $m^{-3}$) were present. The southern section remained below 3 mg $m^{-3}$ (Figure 17). These results align with existing literature. Large phytoplankton blooms in Lake Tanganyika are rare but typically occur in September or October at the onset of the wet season, particularly in the northern region (Cocquyt et al., 2021). Such blooms are driven by seasonal upwelling, caused by trade winds from the south that shift the thermocline. When the winds subside, nutrient-rich deep waters rise, fuelling blooms. The prominence of the 2018 event may be linked to unusually strong trade winds. Turbidity was generally high (>1 FNU), peaking at 5.9 FNU in areas with high Chl-a, while the lowest values were found near the lake's western center, close to the River Lukuga outflow.

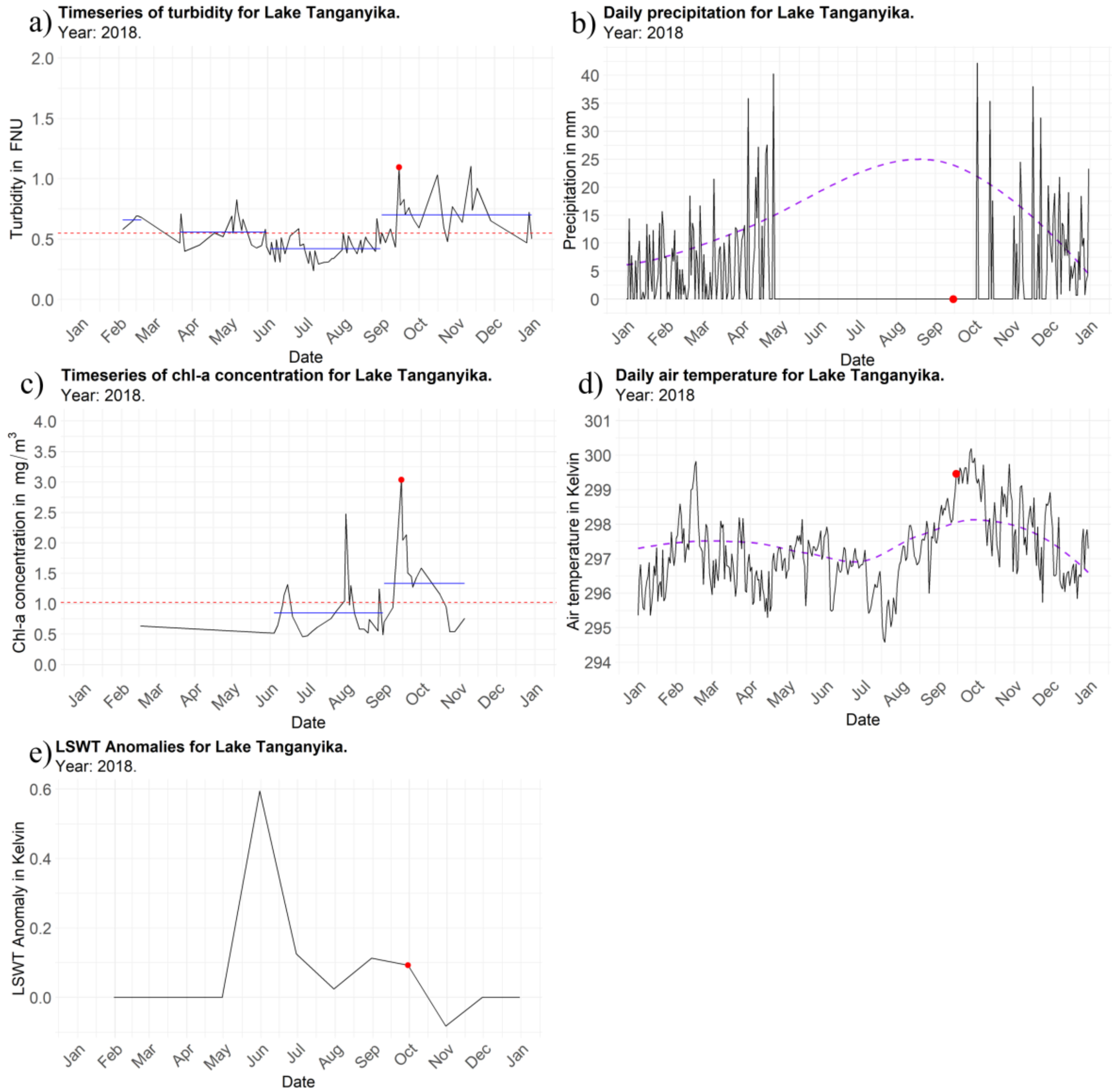


Figure 16. Meteo climatic and water quality parameters linked to the selected extreme event for Lake Tanganyika in 2018. a) Timeseries of turbidity. b) Timeseries of daily precipitation. The purple dashed line shows the lowess line for daily precipitation in 2016-2020. c) Timeseries of Chl-a concentration. The dashed red line is the mean of the year. The blue solid line is the seasonal mean. d) Timeseries of daily air temperature (t2m). The purple dashed line shows the lowess line for daily air temperature in 2016-2020. e) Timeseries of LSWT anomalies calculated are displayed for the last day of the month.

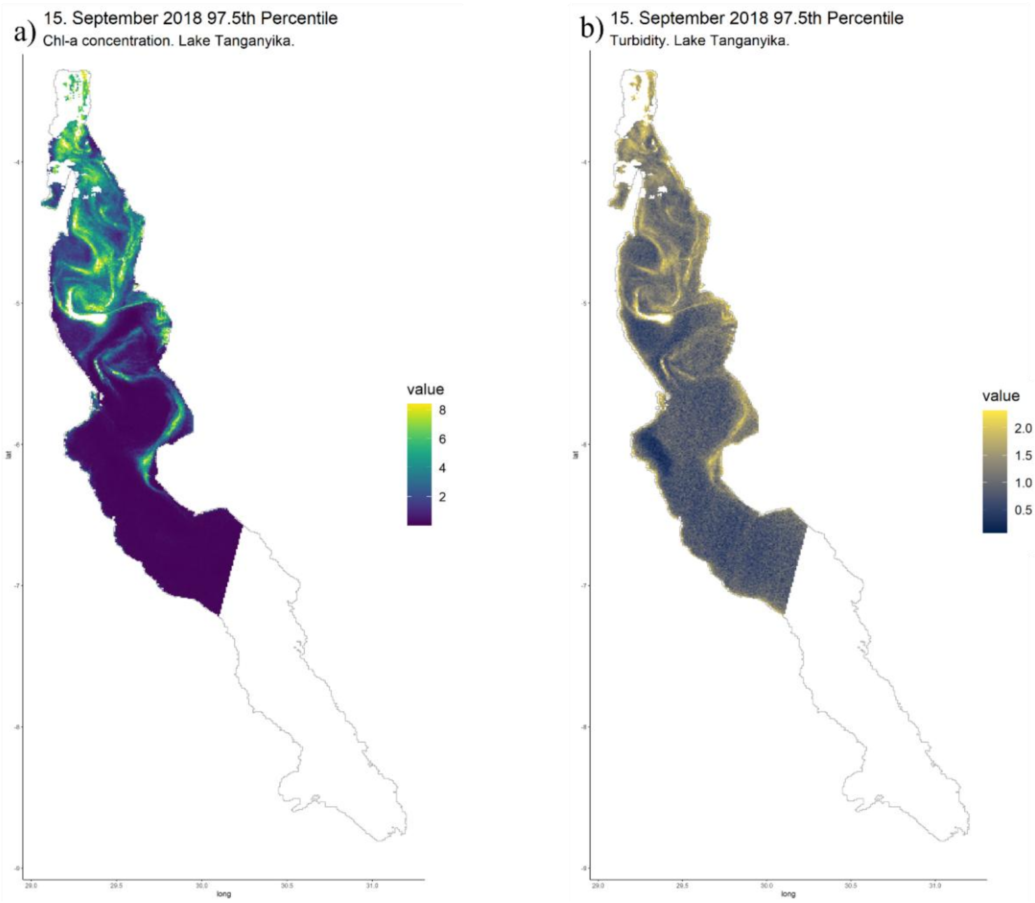


**Figure 17. Maps of Chl-a concentration (a) and turbidity (b) for the compound extreme event on 15/09/208 in the northern half of Lake Tanganyika.**

**Climate–Water Quality Relationships**

Significant correlations between meteo-climatic and water quality variables were observed across all studied lakes (Figure 6). Key relationships include:

- Precipitation and turbidity in Lakes Kariba and Tanganyika.
- Precipitation and Chl-a in Lakes Kariba and Volta.
- Precipitation and LSWT in Lakes Tanganyika, Kariba, Kyoga, and Volta.
- Air temperature and LSWT in Lakes Turkana, Kariba, Naivasha, and Volta.
- Air temperature and Chl-a in Lakes Turkana and Kariba.

Although some correlations were not statistically significant (e.g., precipitation and turbidity in 4 out of 6 lakes, precipitation and Chl-a in 4 lakes, LSWT and turbidity in all 6 lakes), the robustness of the correlation analysis suggests that these links cannot be entirely dismissed. These patterns support the notion that extreme events are likely drivers of lake water quality degradation, in line with previous research (Havens et al., 2016; Khan et al., 2015; Zeman-Kuhnert et al., 2022). A more targeted approach, focusing solely on data from identified compound extreme events, would enhance statistical power. However, the current dataset includes at most two similar events per lake, which limits such analysis. Future studies should prioritize the collection of more compound event data and consider multivariate approaches to better understand the interplay between climatic drivers and biophysical responses.

Table 6. Summary of the correlation between meteo-climatic and water quality variables during the EE identified for the six studied lakes. *** p < 0.001; ** p < 0.01; * p < 0.05; Ka = Lake Kariba, Ky = Lake Kyoga, Na = Lake Naivasha, Ta = Lake Tanganyika, Tu = Lake Turkana and Vo = Lake Volta

| | tp | t2m | LSWT | Chl-a | Turbidity |
|---|---|---|---|---|---|
| tp | | | | | |
| t2m | R = -0.63 *** Ky;<br>R = -0.19 *** Vo | | | | |
| LSWT | R = 0.81 *** Ta;<br>R = 0.81 *** Ka;<br>R = 0.49 ** Ky;<br>R = 0.45 * Vo | R = 0.48 *** Tu;<br>R = 0.79 *** Ka;<br>R = 0.7 *** Na;<br>R = -0.4 * Vo | | | |
| Chl-a | R = 0.58 *** Ka;<br>R = 0.67 ** Vo | R = -0.43 ** Tu;<br>R = 0.5 ** Ka | R = 0.62 *** Ka;<br>R = 0.61 ** Vo | | |
| Turbidity | R = 0.53 *** Ka;<br>R = 0.65 *** Ta | R = 0.59 ** Ta;<br>R = -0.68 *** Vo | R = 0.65 *** Ta,<br>R = 0.69 *** Ka;<br>R = 0.72 *** Vo | R = 0.41 * Ta;<br>R = 0.62 *** Ka;<br>R = -0.35 ** Tu;<br>R = 0.59 ** | |

In summary, in most extreme event cases, clear relationships were found between precipitation and turbidity and Chl-a, as well as between air and water temperatures and Chl-a, consistent with previous research. These patterns suggest that compound extreme events contribute to the degradation of lake water quality. However, the interactions between meteo-climatic and water quality variables are complex and interconnected, making it difficult to isolate the effects of individual drivers. As extreme events are expected to intensify, understanding these interdependencies becomes increasingly important. To better capture spatial variability during compound events, Chl-a and turbidity maps from Lakes_cci (based on Sentinel-3 at 300 m resolution) can be combined with higher-resolution Sentinel-2 imagery (up to 10 m). This approach enhances the spatial interpretation of water quality responses within each lake.

## 5.4 Extreme Weather Effects on Sub-Sahelian Inland and Coastal Lakes

An additional step in the previous study involved extending the analysis to include the effects of extreme weather events on both inland and coastal waterbodies. This extension was motivated by the limited attention previously given to coastal inland waters included in the Lakes_cci dataset. This second part of the study focused on identifying extreme weather events and climate patterns in a selection of coastal waterbodies, with particular emphasis on the differences between inland lakes and coastal lakes or lagoons. The objectives of this study are to: i) investigate time series and patterns of meteo-climatic and water quality variables using modelled and satellite remote sensing data; ii) identify and analyse specific compound extreme events between these variables during the 2016–2020 period; and iii) explore potential differences between inland and coastal waterbodies. The methodology was the same described in the section 5.3.1. In this analysis, 12 coastal lakes and lagoons were examined, and the results were compared with those obtained for the inland lake subset (Figure 18).

Pattern analysis revealed that both inland and coastal lakes experienced increased rainfall over the five-year period, while air temperature remained largely stable. Notably, LSWT showed greater variability in inland lakes compared to coastal ones. Coastal lakes generally exhibited declining Chl-a concentrations, whereas increases were more common among inland lakes. In contrast, turbidity tended to rise more in coastal lakes than in inland ones.

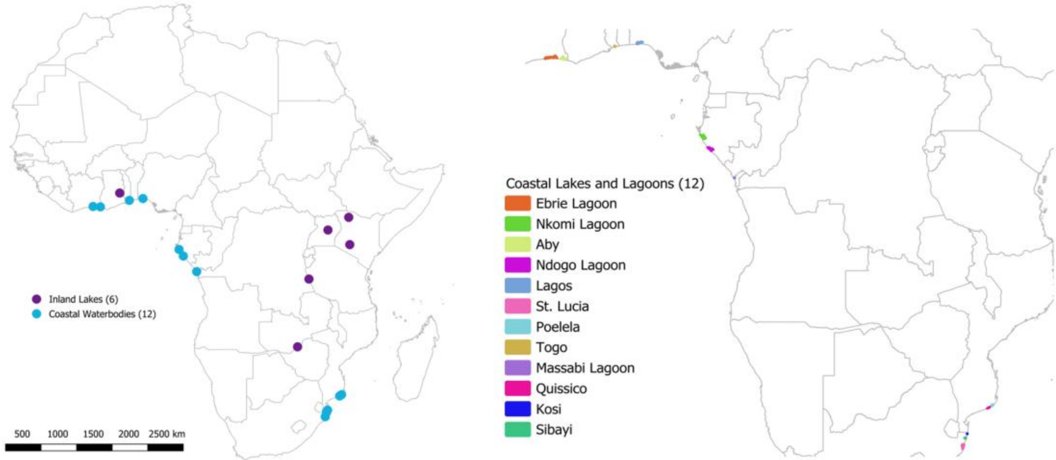


Figure 18. Inland and costal waterbodies selected for this study.

Table 7. Overview of patterns (yearly aggregation) for the meteo-climatic and water quality variables in the period 2016-2020. In purple inland lakes and in blue coastal lakes or lagoons.

| Lake | Precipitation | Air temperature | LSWT | Chl-a | Turbidity |
|---|---|---|---|---|---|
| Volta | ↓ | - | ↓ | ↓ | ↓ |
| Turkana | ↑ | - | ↑ | - | - |
| Kyoga | ↑ | ↓ | ↓ | ↑ | ↓ |
| Naivasha | ↑ | - | ↑ | ↑ | ↑ |
| Tanganyika | ↑ | - | - | - | - |
| Kariba | - | - | ↓ | - | ↑ |
| Ebrie | ↑ | - | - | - | ↑ |
| Nkomi | ↑ | - | - | - | ↑ |
| Aby | ↑ | - | - | ↓ | ↑ |
| Ndogo | ↑ | - | - | ↑ | - |
| Lagos | ↑ | - | - | - | ↓ |
| St. Lucia | ↓ | - | - | ↓ | ↑ |
| Poelela | ↓ | - | - | ↓ | - |
| Togo | ↑ | - | - | - | ↓ |
| Massabi | ↑ | - | - | ↑ | - |
| Quissico | ↓ | - | - | ↓ | - |
| Kosi | ↓ | - | - | - | - |
| Sibayi | ↓ | - | - | ↓ | ↑ |

In synthesis, a total of 25 compound extreme events were identified in inland lakes, compared to 148 events detected in coastal waterbodies for the period 2016-2020. As an example, Figure 19 shows a compound extreme event that was identified for Lakes St. Lucia on 05/01/2020, when precipitation and turbidity showed $Z$-score > 3.9 and 2.5 respectively. Mean precipitation were 22.3 mm and turbidity of 31.1 NTU.

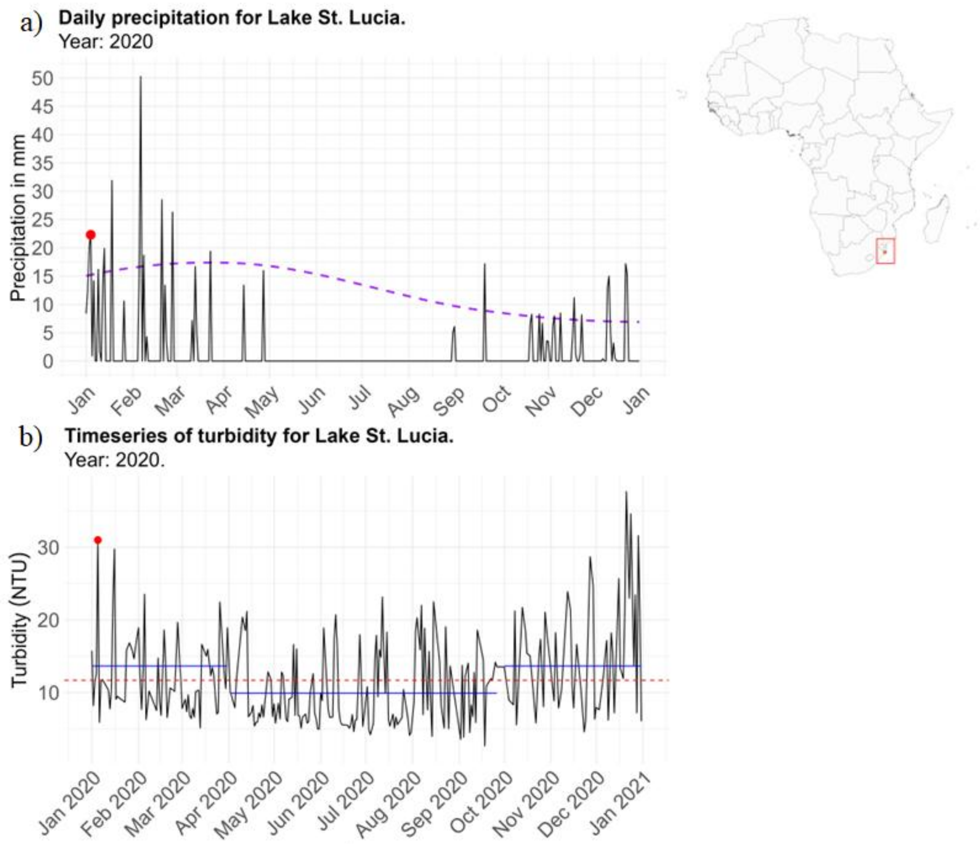


**Figure 19. Timeseries of daily precipitation (a) and turbidity (b) for the selected extreme event for Lake St. Lucia in 2020. In purple the lowess line for daily precipitation in 2016-2020. The dashed red line represents the mean of the year. The blue line represents the seasonal mean.**

In inland lakes, significant positive correlations were found between air temperature and both LSWT and Chl-a, LSWT and Chl-a, as well as precipitation with turbidity and Chl-a. In coastal waterbodies, air temperature was significantly correlated with LSWT and turbidity, while precipitation showed strong positive correlations with both turbidity and LSWT, and LSWT was also positively correlated with turbidity

In this second part of the study a further step was the application of the Principal Component Analysis (PCA) to identify clusters of climate regulators. We apply a PCA to reduce six atmospheric variables into two Principal Components (PCs) that capture the most variance. The results for LSWT, Chl-a, turbidity and lake water level (LWL; when available in Lakes_cci dataset) correlation with PC1 and/orPC2 are reported for the six inland lakes in Figure 20, and for the 12 coastal waterbodies in Figure 21.

From the analysis carried out on the selected African lakes it is evident that rain and shortwave radiation are the main driver in the majority of inland lakes investigated, while wind and Rain&SW$_{down}$ are the main factors in the coastal lakes. From our finding, we can also preliminary highlight a common negative relationship between LSWT and rainfall (e.g., Turkana, Kyoga, and Nkomi lagoon), and a positive relationship between turbidity and rainfall (e.g., Tanganyika, Kariba, Nkomi, Togo), and a general correlation with Rain&$SW_{down}$, while a more complex and weakly interaction between Chl-a and the weather variables, except for example a clear negative relationship with wind in Lake Volta.

In summary, from this pilot study we obtained interesting first insight of the complex relationship between climate variables and lake response in terms of bio-physical variables. EO-derived data are crucial observation to support this long-term and spatial analysis at a continental and global scale. A general risk of water quality deterioration was revealed in the context of the observed extreme weather events.

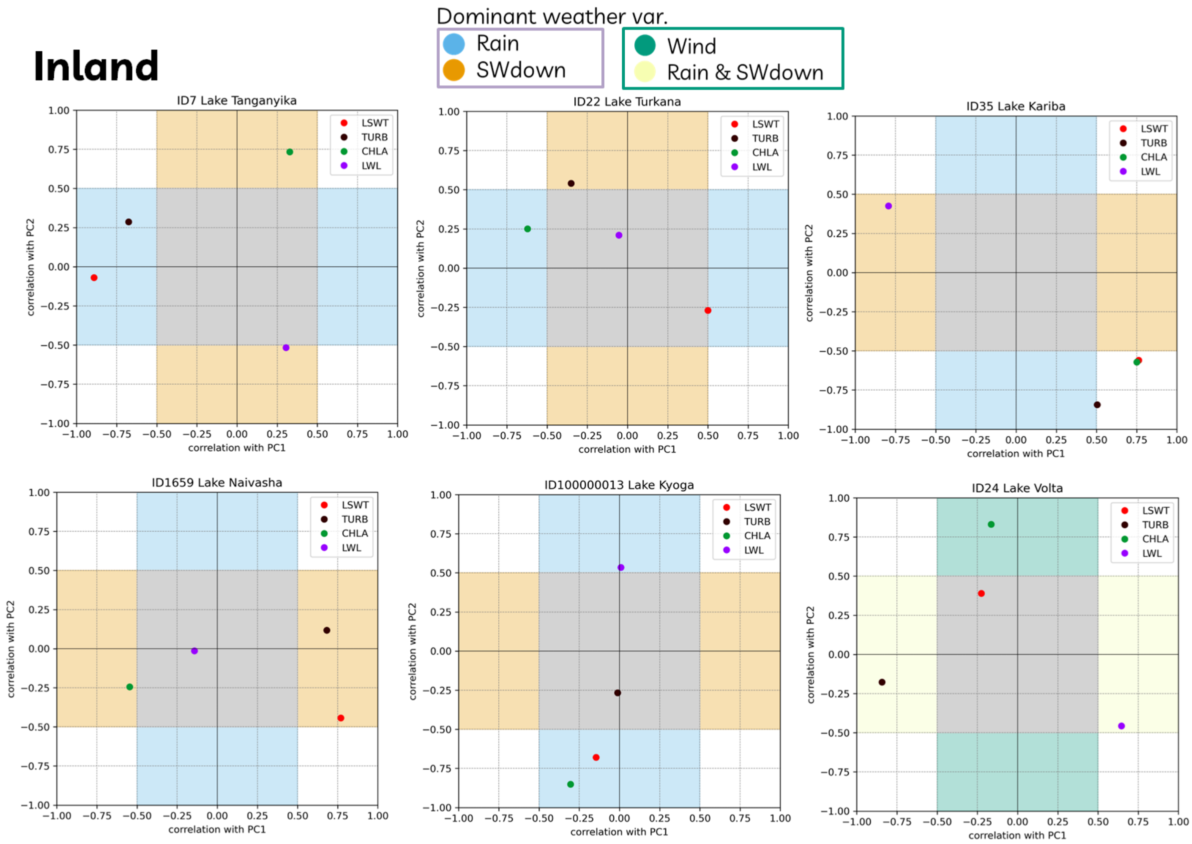


Figure 20. Principal component analysis graphs for the six inland lakes. The weather variables (Rain, Shortwave radiation ($Sw_{down}$), Wind, Rain& $Sw_{down}$) are identified by the colour of the vertical band as PC1 and by the colour of the horizontal band as PC2. The coloured shadowed bands represent the areas where the lake variables are weakly or not correlated with PC1 (vertical band) or PC2 (horizontal band).

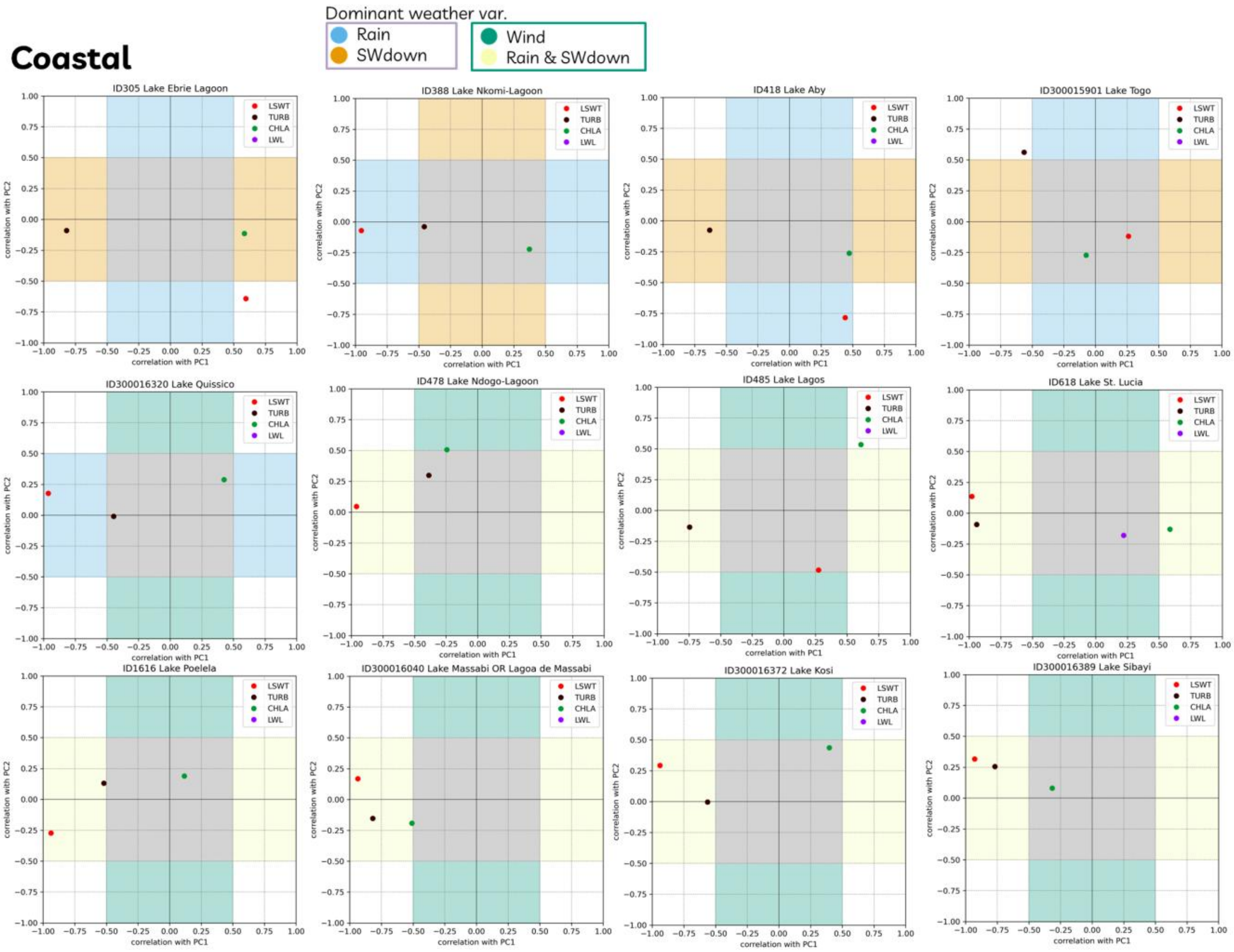


Figure 21. Principal component analysis graphs for the 12 coastal lakes. The weather variables (Rain, $Sw_{down}$, Wind, Rain& $Sw_{down}$) are identified by the colour of the vertical band as PC1 and by the colour of the horizontal band as PC2. The coloured shadowed bands represent the areas where the lake variables are weakly or not correlated with PC1 (vertical band) or PC2 (horizontal band).

# 6 Use cases

## 6.1 Heatwave and storm event impacts on lakes

Recent projections estimate that increases in the duration, intensity, and spatial extent of heatwaves over most land regions are expected. The IPCC predict that warming is set to continue with an over 90% likelihood of a continuation of the increase in the frequency of heat extremes over the 21st century, especially in southern regions (Ranasinghe et al., 2021). In the context of climate change, the impact of extreme climate events such as heatwaves, demonstrates the vulnerability of lake ecosystems to climate variability, with waters getting warmer for longer periods (Woolway et al. 2021).

In relation to the use cases selection within the CCI dataset, we focused our investigation of the effects of heatwaves on lake water quality in two different continent, Europe and India.

In Europe the trend toward a warmer and drier climate has been underway for several decades and the increase in heatwaves frequency has been associated with the reduction in Arctic Sea ice and Eurasian snow cover, a process likely to continue during the next century (Zhang et al. 2020). In the summer of 2019, a double heatwave event occurred in Europe resulting in one of the warmest summers since 1500 (Sousa et al., 2020) and we investigated responses on 36 selected lakes using Lakes_cci Chl-a estimates and total phosphorous data (from Waterbase daset of the European Environment Agency). Results have been presented in the previous CAR report (version January 2024) and published in a peer-reviewed paper (Free et., al 2022).

The study in European lakes, detailed in Free et al. (2022), concluded that timing and magnitude of the response to the heatwave events depends on lake depth and nutrients. Deeper lakes respond sooner, probably because of higher temperatures leading to stronger stratification, thereby improving the light climate but with the response strength dependent on nutrient status. This was supported by lakes at higher latitudes, typically colder, showing greater synchrony between air temperature and Chl-a. In contrast, shallower lakes and lakes at lower latitudes showed more asynchrony responses of Chl-a, typically after heatwave events as a result of internal and external loading. Following on from these conclusions, further work investigated the responses of lake water quality to rising temperatures during heatwaves and to low-pressure events at the end of heatwaves in other continents.

India is one of the global hot spots experiencing severe heatwaves, with an increasing number of mega heatwaves recorded since the beginning of the century (Hari et al., 2022; Vittal et al., 2020; Rohini et al., 2016). The occurrence of heatwaves over the Indian subcontinent is mostly associated with high-pressure systems characterized by anticyclonic wind patterns and sinking air which prevents cloud formation, with subsequent clear sky conditions, intense surface heating and decreased soil moisture (Ratnam et al., 2016; Zore et al., 2021). The Indian climate is strongly dominated by the monsoon, the timing and intensity of which is increasingly subject to climate change. In 2019 the monsoon was delayed and preceded by a significant heatwave.

**In the Indian sub-continent, we examined satellite derived estimates of lake turbidity and chlorophyll-a (Chl-a) from the CCI dataset, during year 2019 for 42 lakes and reservoirs, to investigate the potential responses to the occurrence of heatwaves and monsoon. The 42 lakes were located in the region extending from 10°N to 34°N, from 70° E to 87° E, hence representing significant latitudinal and longitudinal gradients across multiple ecoregions, from humid subtropical to arid to highlands (**

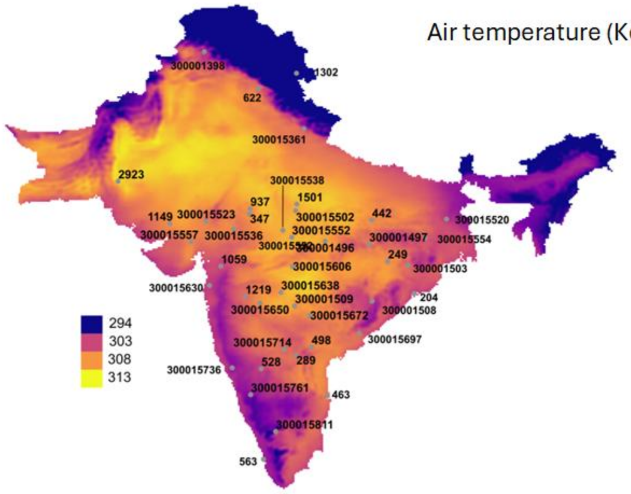


Figure 22). The lake types were mainly reservoirs (33), with only 9 natural lakes.

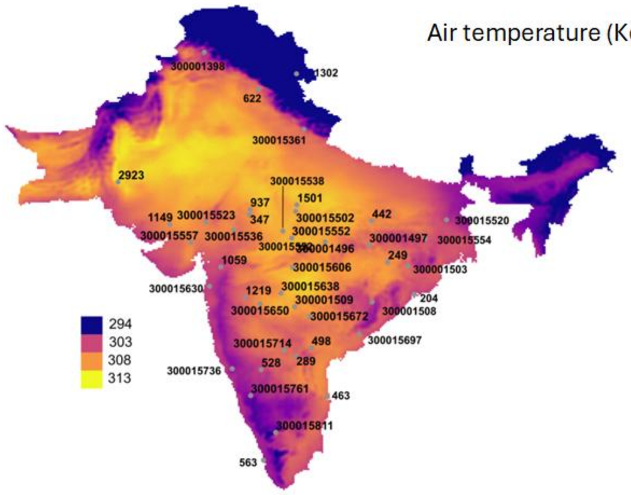


**Figure 22. Maps of India with the selected lakes distribution and air temperature (Kelvin) in 2019 (a) during the heatwave (1st June) and (b) during the monsoon period (18th July).**

Cluster analysis of annual patterns of lake turbidity and Chl-a concentrations during 2019 provided insights into lake responses to heatwave and monsoon periods. Three main clusters were identified for Chl-a concentration and two main clusters for turbidity concentration. Figure 23 shows Chl-a (**a-** in green) and turbidity (**b-** in brown) annual patterns (relativised to the mean) for each cluster. Clusters of turbidity patterns were mainly related to precipitation patterns and latitude, while clusters of Chl-a patterns were influenced by lake morphology, phytoplankton dynamics and their interaction with changes in water turbidity.

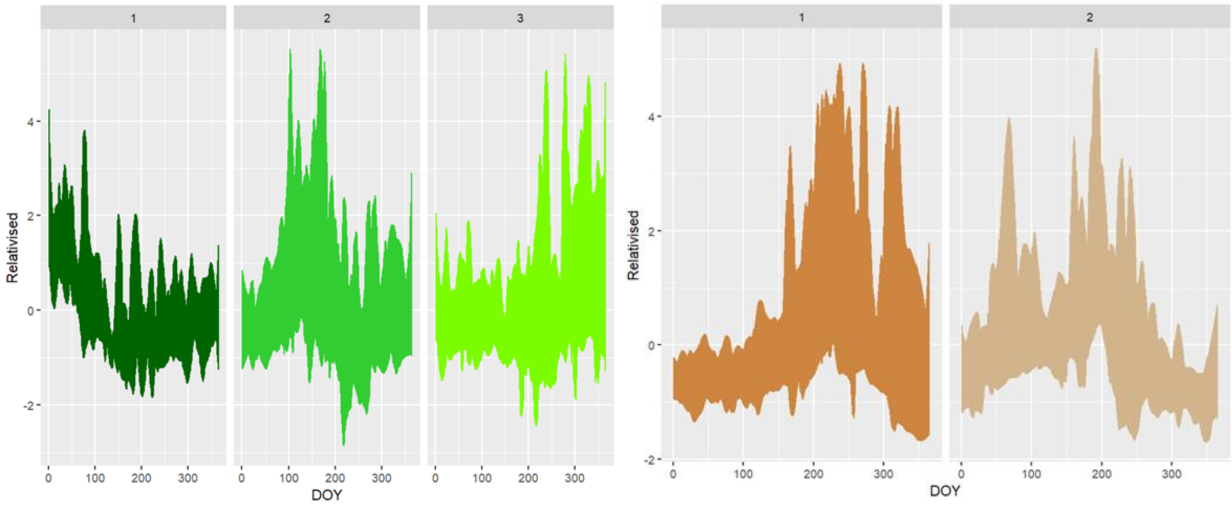


(a) (b)

Figure 23. Lake chlorophyll-a (a) and turbidity (b) (relativised) annual patterns by cluster.

Further analysis in our study revealed that monsoon precipitation was the main driver of turbidity dynamics and resulted patterns in the studied lakes. Time Alignment Measurement analysis showed that the time series of turbidity for the lakes were closer in phase with precipitation indicating the driving influence of monsoon rains. Results from cross-correlation analysis resulted in significant coefficients between the time series of cumulative precipitation and lake turbidity concentration, indicating a general response time lag of one month.

Available data on lake water level indicated that level variation can be high within a short period of time, strongly influencing lake water dynamics and quality. LWL data indicated that 2019 was a particularly severe year for some of the studied lakes; for instance, in Lake Gandhi and Lake Nath the minimum LWL was reached in June 2019 over a four-year period (2017-2020) and corresponded to the highest turbidity concentrations registered in the following period (July-September) when the monsoon rains replenished the water basins.

In conclusions, our studies showed how satellite derived estimates of turbidity and Chl-a represent a feasible method of providing high frequency and synoptic data, capable of covering large scale weather events at continental scale (*Caroni et al., "A remote sensing approach for characterizing lake responses to heatwaves and monsoons: a case study from India", submitted to IWA Publishing*). Both studies in Europe and India revealed that morphological characteristics of lakes are key factors in the timing and magnitude of responses in water quality variables to heatwave occurrence. In particular, lake mean depth was important for determining Chl-a timing responses and for shaping patterns, with deeper lakes generally showing a more synchronous response to heatwaves than shallower lakes. The main driver of turbidity patterns in India was found to be precipitation, occurring in a continental area with a distinctive dependence of monsoon seasonality.

## 6.2 Water quantity in relation to water quality in a changing environment

### 6.2.1 La Niña influence on water quantity and quality in Lake Qadisiyah, Iraq

Lake Qadisiyah is located on the Euphrates River in the north of Iraq, it was created after the construction of the Hadithah dam in 1977, with the purpose of regulating runoff from the Euphrates River, providing irrigation for local fields, producing hydroelectricity, and partially controlling floods (Kamnev and Malyshev, 1983). The Hadithah dam is the second largest dam in Iraq and regulates the Euphrates River for the whole country (UNEP, 2017). The designed normal water level of the dam is 143 m with a storage of 6.4 $km^3$ (Kamnev and Malyshev, 1983) and the surface area of the lake is 428 $km^2$. Because of locating in a semi-arid region and the cross-boundary Euphrates River feature, water in this lake is affected by both climate and human activities.

We used the lake water level (LWL), Chlorophyll-a concentration (Chl-a), and turbidity products from the ESA Lakes_cci dataset covering the period of 2000–2019 in this lake, to study the water level and water quality changes in the past 20 years, and their relationship. We collected the precipitation, wind speed and air temperature data in the lake catchment from the ECMWF ERA 5 dataset, the standardized precipitation index (SPI) expressing drought in the lake catchment from Copernicus Emergency Management Service, the bi-monthly El Niño/Southern Oscillation (MEI) data from National Oceanic and Atmospheric Administration (NOAA), the land use and land cover (LULC) type in the catchment from MCD12Q1, land surface temperature from MOD11A2, and the normalised difference vegetation index (NDVI) data from MOD13A2 for the same period (2000-2019), to investigate the driving factors of water quantity and quality changes in this lake.

Results showed that the average water level of this lake was 138.3 m in 2000-2019, it decreased clearly in 2001, 2009, 2015 and 2018 with the lowest value of 120 m in July 2015 (Figure 24). The mean Chl-*a* was 6.3 $mg/m^3$ and it showed an overall increasing trend during 2000 and 2019. Turbidity showed extremely high values (>10 NTU) in 2009 and 2017-2018 compared to the mean value of 3.6 NTU in 2000-2019. An overall negative relationship was observed between water level and water quality (Chl-*a* and turbidity).

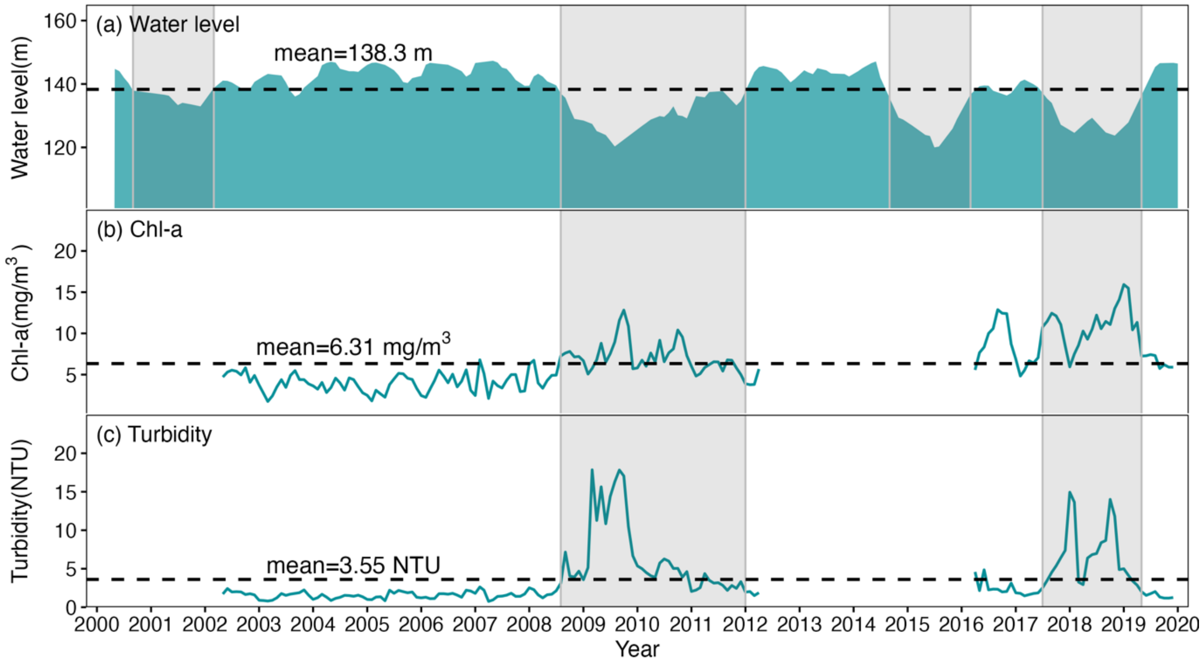


Figure 24. Changes of water level, Chl-a concentration and turbidity during the period 2000–2019 in Lake Qadisiyah, Iraq. Grey shaded areas indicate water levels lower than the average in the past twenty years. Black dashed lines are the mean values of water level, Chl-a concentration and turbidity during 2000–2019.

The boosted regression tree (BRT) was then used to explore the relationship between those variations and El Niño-Southern Oscillation, droughts, meteorological factors and LULC changes in the catchment. Results revealed that water level declines were mainly associated with droughts (SPI) led by La Niña events. While MEI explained 67.5% of SPI variations in the Lake Qadisiyah catchment, and showed a significant negative relationship ($p<0.01$) (Figure 25a). Lower SPI values normally appeared when MEI was low, which means La Niña coincided with drought events in the lake catchment. Precipitation was the second most important factor but only contributed 18.6% to SPI variations in the catchment, with low SPI values (drought) occurring when precipitation was low (Figure 25b).

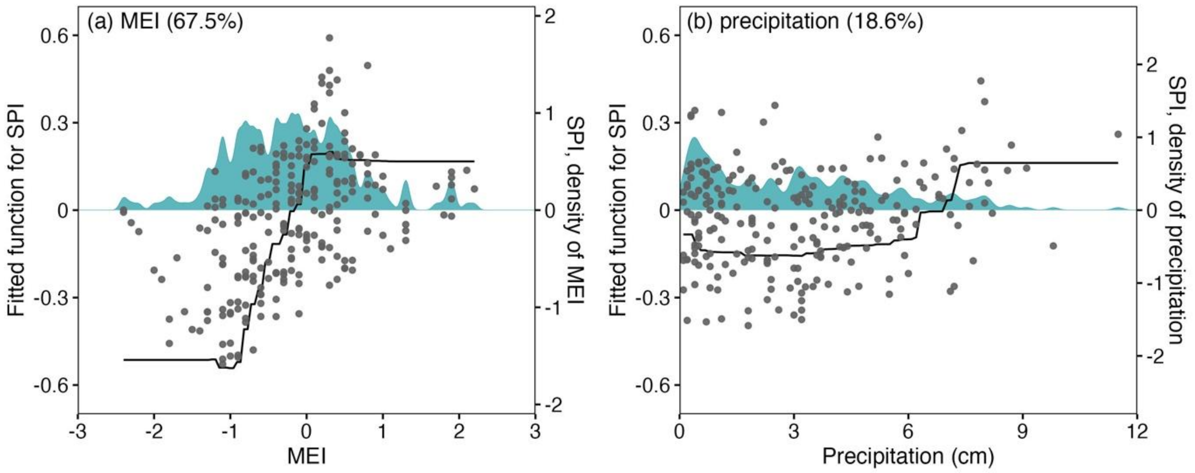


Figure 25. Impacts of (a) MEI and (b) precipitation on drought events in the Lake Qadisiyah catchment. The solid line is the fitted function of MEI or precipitation on drought events, grey dots are the monthly SPI and teal area is the density of MEI or precipitation during 2000 and 2019.

Chl-*a* increase in the lake were mainly explained by built-up area increase and water area decrease in the catchment, with a relative contribution of 29.2% and 28.6% respectively (Figure 26a,b). Water area changes in the catchment were the main factor influencing turbidity explaining 55.3% of the variation (Figure 26c and d).

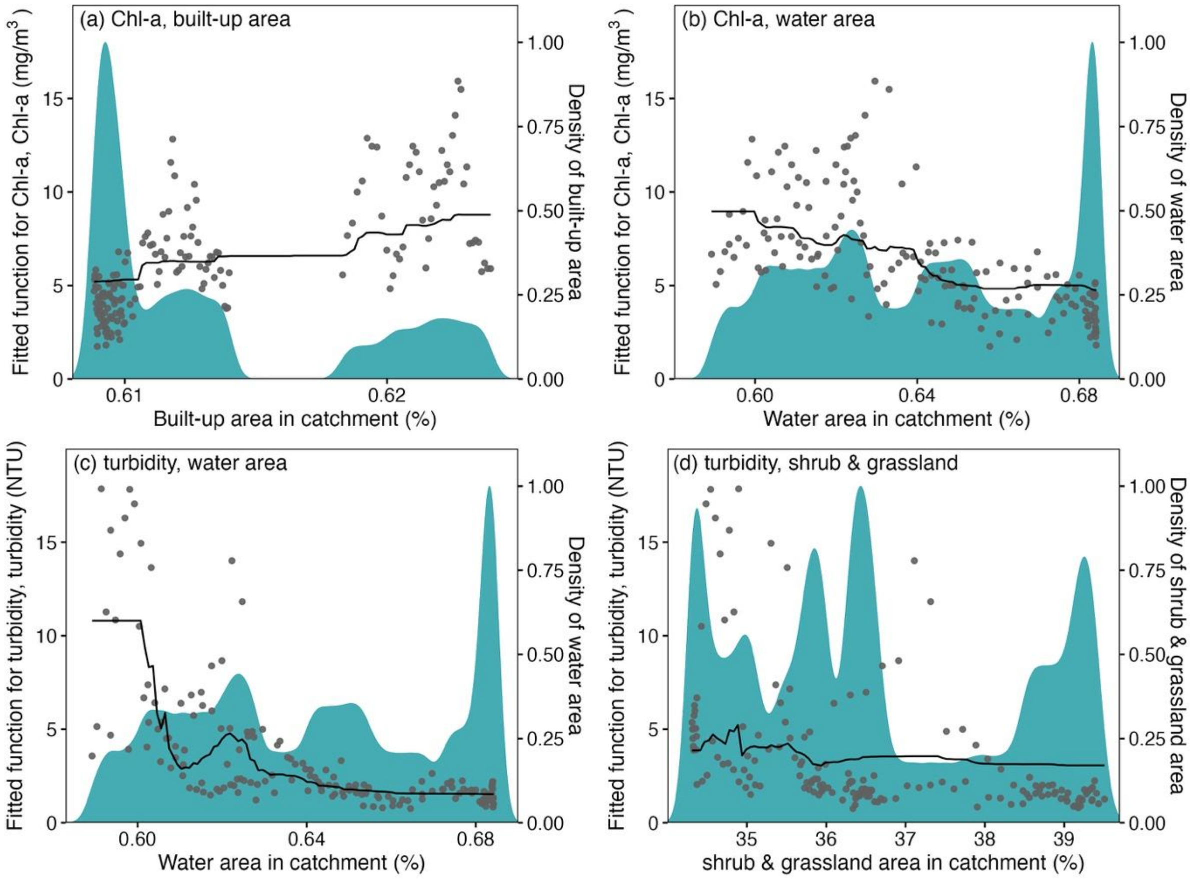


**Figure 26. Relationship between (a) built-up area, (b) water area in the catchment and Chl-a in Lake Qadisiyah. Relationship between (c) water area, (d) shrub & grassland area in the catchment and turbidity in Lake Qadisiyah. Solid lines are the fitted functions of factors on Chl-a or turbidity variations. Dots are the monthly Chl-a or turbidity. Teal areas are the density of each factor in the graph.**

An exception of water level decline in 2014-2016 was also observed when there was no drought, and the precipitation in the catchment did not show large anomalies in 2014–2016. NDVI can indirectly reflect water availability in the catchment as vegetation is sensitive to drought in semi-arid area (Barlow et al., 2016; Daham et al., 2018). However, NDVI did not show any decrease in the year of 2014–2016 (Figure 27). The reported military conflicts with water flow cut off in upstream from March to October 2015, and water release from the Haditha dam with a result of water area increase in downstream of Lake Qadisiyah in 2014 (UNEP, 2017; Hasan et al., 2019) seem to explain the observed water level decrease in 2014-2016. The timeline of water flow cut off in upstream matches very well with the time of observed lowest water level in July 2015.

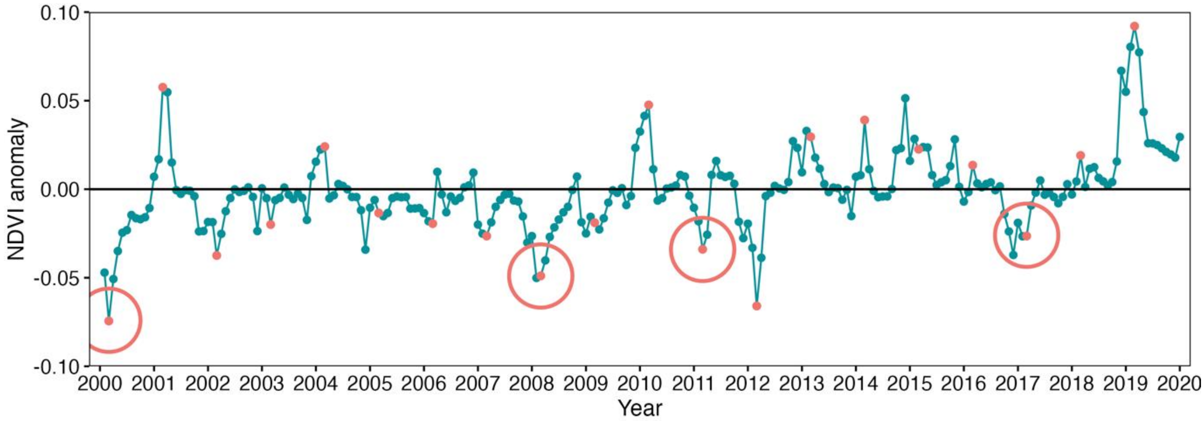


**Figure 27. NDVI anomalies in Lake Qadisiyah catchment. Red points represent NDVI in March, the four red circles indicate the four drought events between 2000 and 2019.**

The analysis and results of this study in Lake Qadisiyah have been published in *International Journal of Applied Earth Observation and Geoinformation* (https://doi.org/10.1016/j.jag.2024.104021).

## 6.2.2 Water quantity and quality variations in lakes globally

The water level-water quality (turbidity) variation and relationship analysis were applied to lakes globally using the available data in the Lakes_cci dataset. The first analysis was carried out for lakes globally using the GAM fitted water level and turbidity time series data. Results showed that for interannual variations, 80% of the lakes (41 out of 51) showed a negative relationship between water level and turbidity (Figure 28).

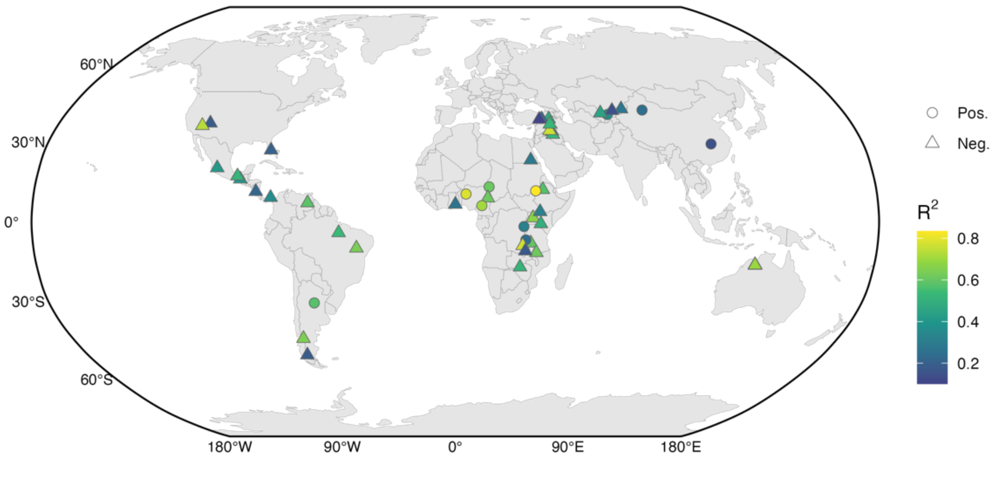


**Figure 28. Relationship between lake water level and turbidity interannual variations for lakes globally.**

Most of the large interannual and seasonal water level changes are found in smaller lakes rather than in big lakes. For instance, 47% of the reservoirs have interannual water level changes larger than 10 m, and 53% of the reservoirs have seasonal water level changes larger than 5 m (Figure 29).

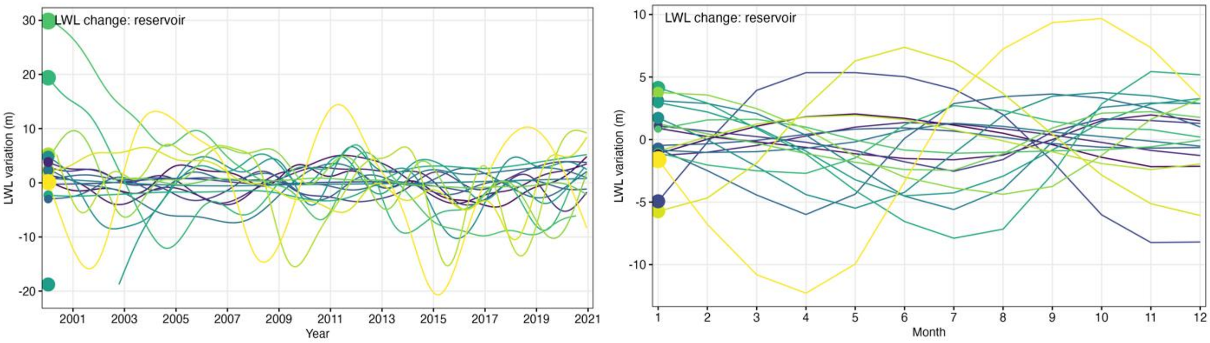


Figure 29. Water level variations across (left) different years, and (right) different months in reservoirs.

A second analysis was carried out focusing on water level and turbidity relationship in reservoirs, as the water level variations of these water bodies are the most significant. In terms of interannual variations, 86% of the reservoirs have negative relationships between water level and turbidity (Figure 30). Only 3 reservoirs showed positive relationship, which are Kainji (Nigeria), Roseires (Sudan), Kayrakkumskoye (Tajikistan). In terms of seasonal variations, 86% of the reservoirs have negative relationships between water level and turbidity. 3 reservoirs, Argyle (Australia), Sakakawea-Audubon (US) and Mosul (Iraq), showed positive relationships between water level and turbidity.

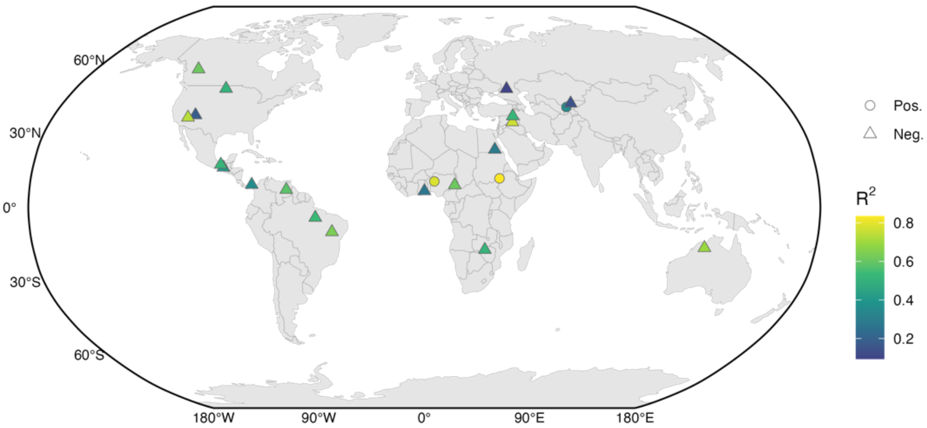


Figure 30. Relationships between lake water level and turbidity interannual variations for reservoirs globally.

Two examples of water level and turbidity relationship are showed in Figure 31. Kainji Reservoir in Nigeria is an example of positive relationship in terms of interannual changes but negative relationship in seasonal variations (Figure 31a). Oppositely, Mosul Reservoir is an example of negative relationship in terms of interannual changes but positive relationship in seasonal variations (Figure 31b).

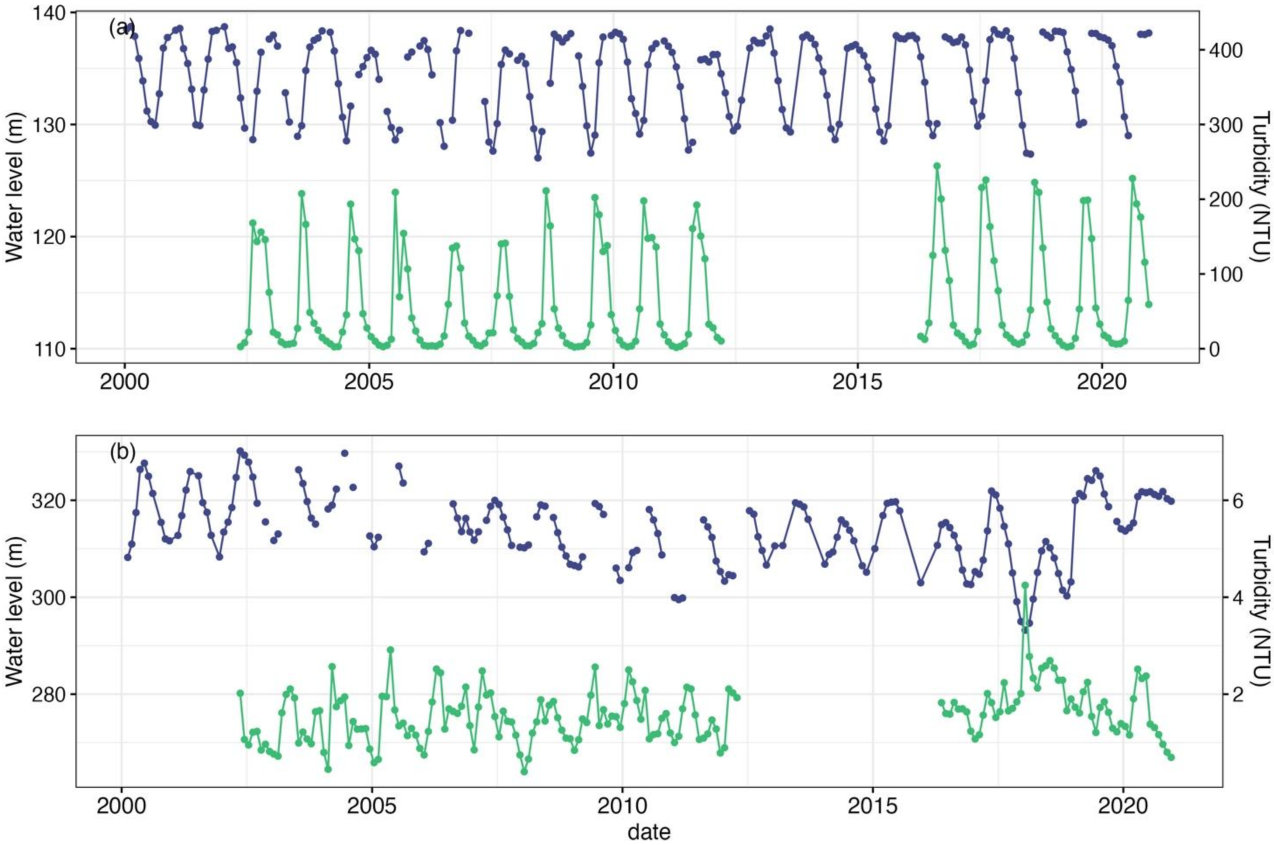


Figure 31. Relationships between water level and turbidity in (a) Kainji Reservoir in Nigeria and (b) Mosul Reservoir in Iraq.

## 6.3 Aggregated climate indicators for the global lakes dataset

Indicators that help to assess climate impacts on lakes were generated based on the Lakes_cci dataset. The initial effort for the climate impact indicator set came from the German Adaptation Strategy (Deutsche Anpassungsstrategie, DAS). This strategy addresses the impacts of climate change in Germany and is designed to help the country adapt and minimize associated risks and vulnerabilities. The strategy was developed by the German Federal Government in response to the growing awareness of climate change and its potential consequences. 120 indicators are defined to monitor and evaluate the state of adaptation and climate change impacts in various sectors, including water quality and management indicators supported by satellite observation. While a national strategy is crucial for understanding and addressing climate change impacts, a global dataset enables other countries to develop those strategies. Here, we focus on the development of lake climate change indicators at the global scale.

In addition to the indicator set, which provide a comprehensive view of trends and vulnerabilities in lakes, a user-friendly visualisation dashboard was developed to make the resulting indicators accessible and understandable to a diverse audience, including policymakers, researchers, and the public. This approach ensures that the insights drawn from the data can be effectively communicated and utilized for informed.

### 6.3.1 Lakes_cci climate indicators

The set of indicators consists of four metrics. It is our objective to expand this set in the future. The indicators were selected because of their high data quality, direct relevance to climate change and relatively high data density. The indicators are based on the Lake_cci CRDP V2.1.0.

#### 6.3.1.1 Temperature anomaly

The first indicator is the temperature anomaly in lakes. This indicator is crucial for understanding variations in lake temperatures, providing valuable insights into the impact of climate change on aquatic ecosystems. By analysing temperature anomalies in lakes, we can assess the thermal health of these ecosystems, which is vital for biodiversity, water quality, and overall environmental resilience. The indicator is calculated on the LSWT data of quality levels 4 and 5 to ensure data reliability. To calculate this indicator, a deseasonalised lake median time series is created. This process removes the influence of seasonal variation, isolating long-term temperature trends. Additionally, the analysis focuses on the five warmest months of the year, selected based on the climatology. Only products with at least 20% valid pixels are used. The final indicator provides a yearly mean of the water temperature anomaly (see example Figure 32).

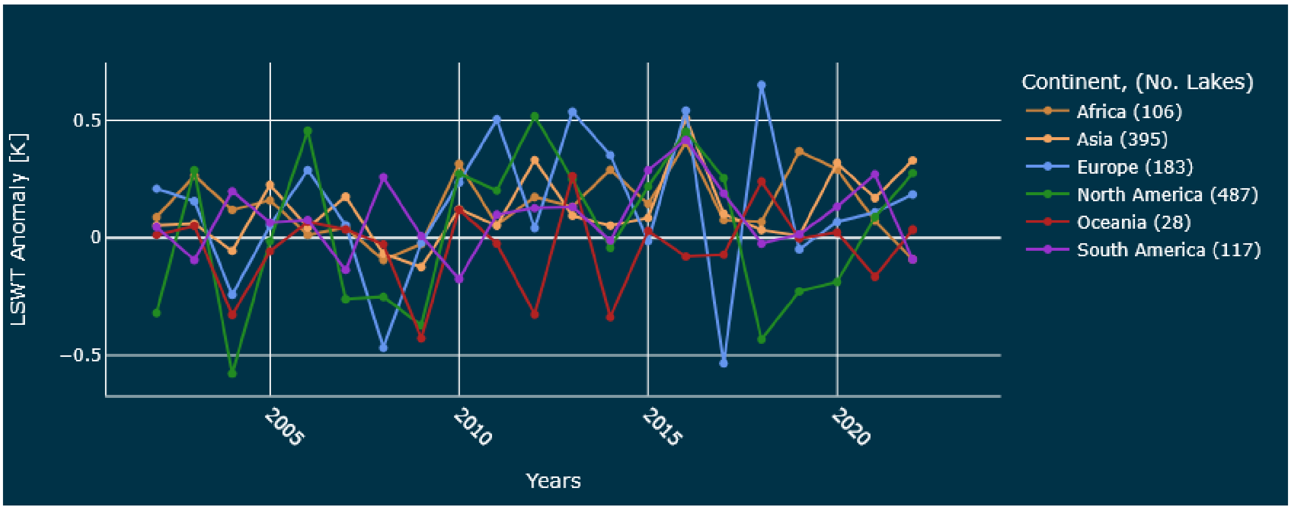


Figure 32. Time series of the lake surface water temperature (LSWT) anomaly aggregated by continent.

#### 6.3.1.2 Heatwaves

The second indicator assesses extreme temperature events in lakes (Figure 33). It follows a methodology similar to the first indicator using LSWT data with quality levels 4 and 5, specifically focusing on the five warmest months of the year and using only daily products with at least 20% valid pixels. A heatwave, is defined here as the lake median temperature exceeding the seasonal 90$^{th}$ percentile of the full time series from 2002-2022, lasting at least two consecutive days within a 5-day period. This methodology follows Hobday et al. (2016) and Woolway et al. (2021). The final metric is determined by counting, per lake, the number of days classified as heat waves, during a given year. This indicator helps us gauge the frequency and intensity of extreme temperature events in lakes, which can have significant ecological and environmental implications.

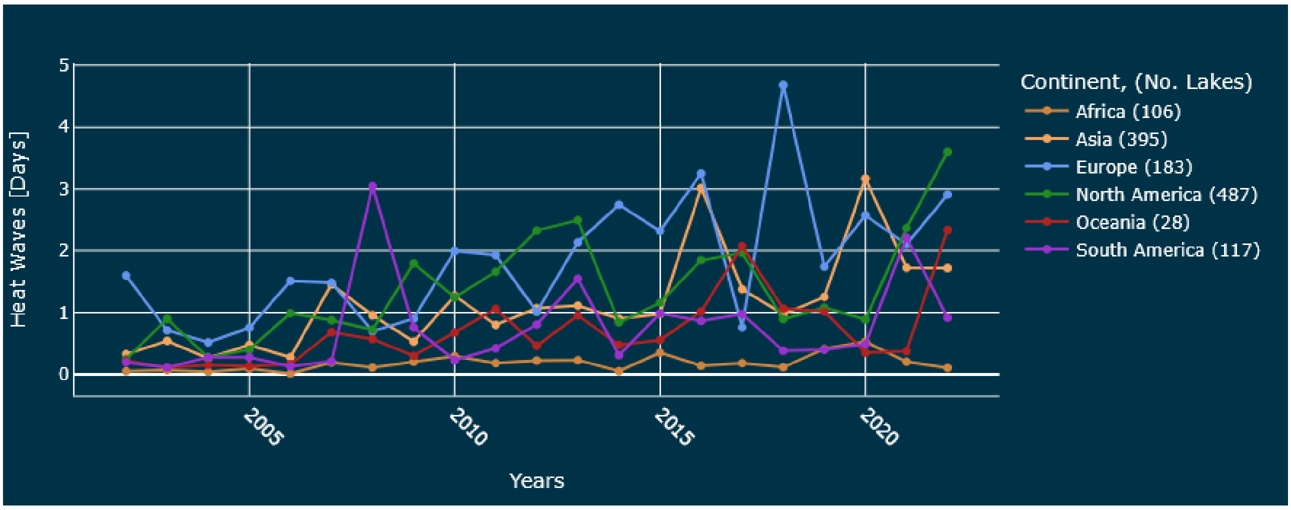


Figure 33. Time series of heatwave-days for the global lakes LSWT data set aggregated by continent.

### 6.3.1.3 Ice cover area

The third indicator is a measure of ice cover in lakes and is calculated by determining the fraction of ice covered pixels in relation to all valid pixels (Figure 34). This means that it quantifies the proportion of the water surface covered by ice during a specific period, irrespective of lake size. The indicator provides insights into the extent and stability of ice in the region of interest. This indicator is valuable for assessing the impact of a changing climate on the presence of ice in lakes, which is significant for various ecological and hydrological processes.

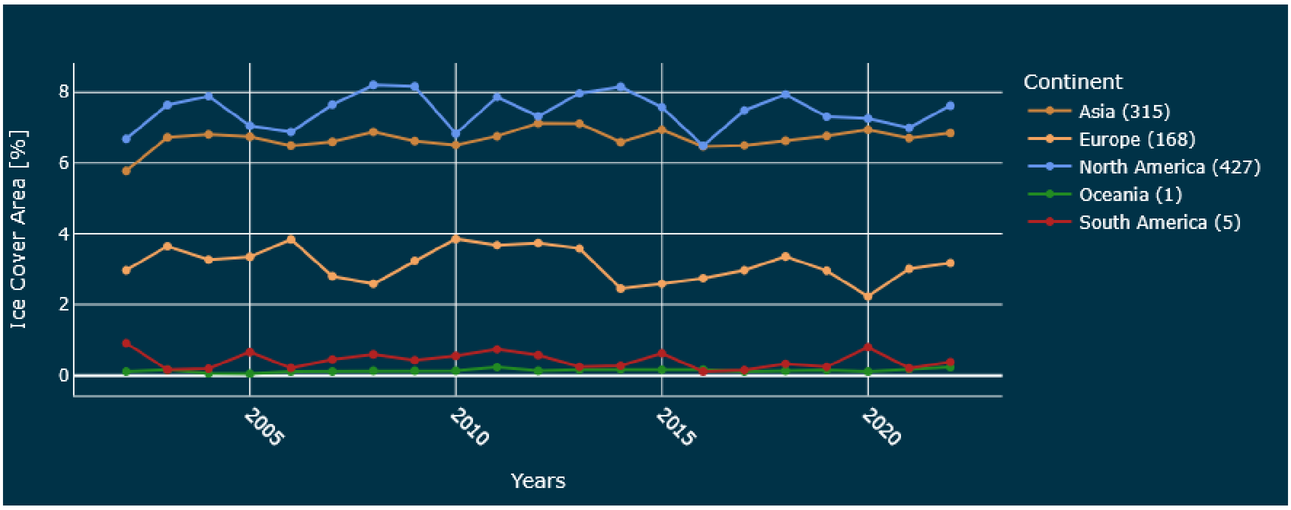


Figure 34. Time series of the global lakes ice coverage area aggregated by continent.

### 6.3.1.4 Ice cover duration

The fourth indicator quantifies the seasonal duration of lake ice cover during the cold period of the year. It estimates the continuous period in which a significant portion of the lake surface is covered by ice.

The start and end of the ice season are determined based on the first occurrence of ice cover before and after the LSWT drops below 278 K. The temperature peak, used as a seasonal reference point, is identified by applying a rolling mean to the annual LSWT time series. In cases where insufficient temperature observations prevent a reliable estimation of the seasonal temperature maximum, a climatological LSWT peak is used as a fallback reference. Only days where at least 30% of the lake surface area is covered by ice are considered valid. Temporary ice melt events occurring between the defined start and end dates are not included in the duration calculation, as the indicator is designed to represent the overall extent of the main ice season. Figure 35 demonstrated the ice cover duration indicator aggregated by continent.

This indicator enables the assessment of interannual changes in ice season length and insight into potential climate-driven shifts.

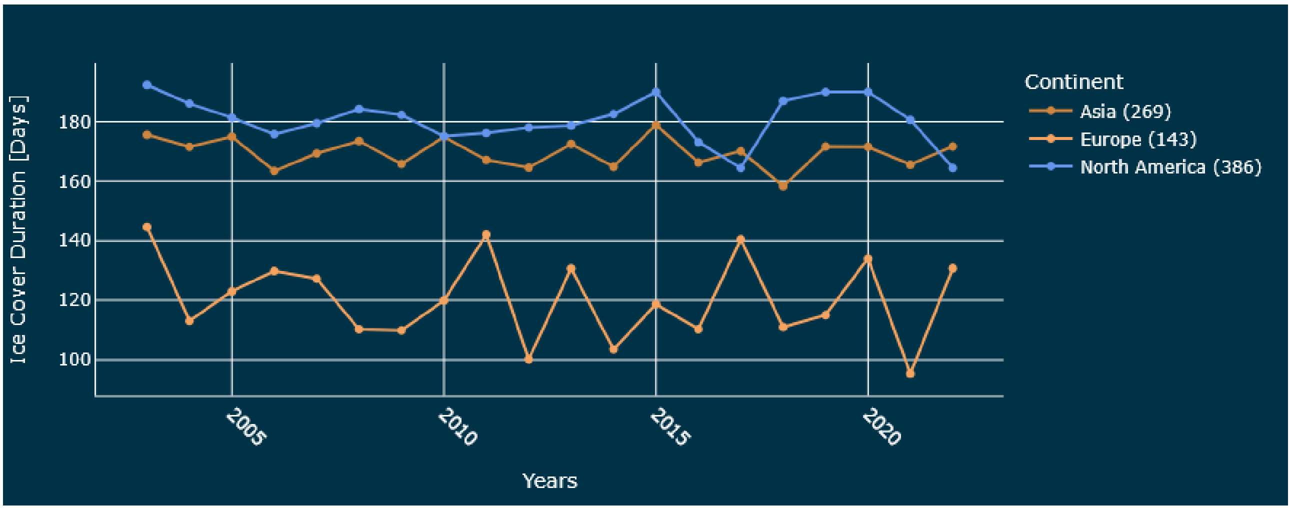


Figure 35. Time series of the global lakes ice cover duration aggregated by continent.

By assessing indicators at the lake level, we gain insights into how individual water bodies respond to climate change, which is critical for understanding ecological impacts and adaptation needs on a local level. Simultaneously, the aggregation of these lake-level indicators into larger properties provides a broader context for a national or global analysis. This approach enables us to identify broader regional or global trends, differences in climate zones, and the influence of lake characteristics on climate change impacts. By leveraging both views, this methodology enhances the overall applicability of our indicators, supporting more informed decision-making and adaptation strategies that can be tailored to specific regions. Lake properties used for the grouping of lakes are collected from the HydroLakes which provides 56 hydrology, physiography, climate and anthropogenic variables. The following aggregation methods are available within the dashboard: continent, lake surface area, lake average depth, climate zone, elevation, population density, annual precipitation, water residence time and lake water volume.

### 6.3.2 Visualisation of climate indicators

A user-friendly browser-based dashboard was developed for easy access to the indicators and their behaviour for different lake groups. The dashboard can be accessed via the following link:

https://lakescci.climate-indicators.brockmann-consult.de/

This dashboard provides an interactive and comprehensive platform for users to explore and understand the indicator results (Figure 36). It features a global map showcasing the spatial distribution of the lakes and incorporates a range of critical information, including time series data, trend analyses, and indicator distributions. Users can select specific indicators and even narrow down their focus to individual countries, making it a versatile tool for anyone interested in tracking indicator development, whether at a global or national level. Additionally, single lakes can be selected in the dashboard and compared to the indicator values of the aggregated levels. This flexibility, coupled with its interactive features, empowers users to gain valuable insights into the impact of climate change and aids in informed decision-making for environmental and climate adaptation efforts.

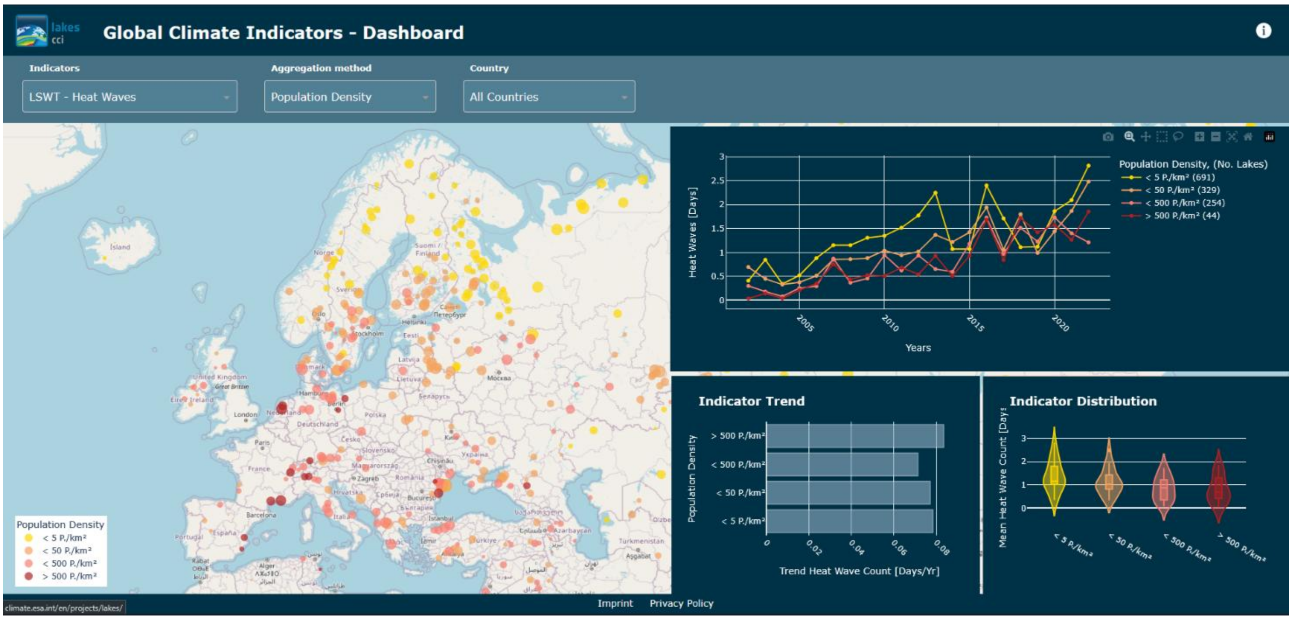


**Figure 36. Overview of browser-based climate indicator dashboard with interactive selection of the indicator, the aggregation method and a country.**

The dashboard not only serves as an analytical tool but is also suitable for raising awareness and promoting the data set to new users. It demonstrates how the data set can be used to understand and address climate change impacts. In addition to its scientific applications, the dashboard is designed to be accessible to non-scientific experts. It offers a user-friendly platform that provides quick overviews of the indicators for lakes, making it a valuable resource for decision-makers, policymakers, and local authorities interested in understanding the state of lakes globally or on a national level in the context of climate change. Thus, the indicators and the dashboard are serving both scientific and policy purposes.

## 6.3.3 Examples

### 6.3.3.1 Lake Ice Cover in Greenland

In Greenland, the dashboard has proven helpful in witnessing the impact of climate change on lake ice cover. The lake ice cover indicator shows a clear and concerning trend. It points to a decrease in lake ice cover, with lakes at altitudes < 1000m showing a decline in ice cover by -30% every 10 years, while a decline is visible also at lower elevations. The geographical location of the lakes, whether they are situated in the northern or southern parts of Greenland, does not seem to be influential in this phenomenon (Figure 37**Error! Reference source not found.**).

The years 2016 and 2019 stand out with low ice cover, whereas a peak was observed in 2009. The lake ice cover indicator demonstrates substantial ice loss during these years. This can be compared to the melt extent of the Greenland ice sheet in 2019, showing an increased melting during this year Temperatures in certain areas of Greenland surged by 10°C above the average in 2019, and at the summit of the ice sheet, which sits over 3,200 meters above sea level, temperatures intermittently exceeded the freezing point for extended periods. Additionally, the months of April, May, June, and July witnessed temperatures consistently surpassing the typical averages across Greenland (Duncombe 2019). While direct comparison between lake ice cover loss and the melting of Greenland ice is not feasible, the findings reveal parallel trends. These observations suggest the potential for utilizing the showcased indicator to pinpoint notable years of fluctuation in lake ice cover areas.

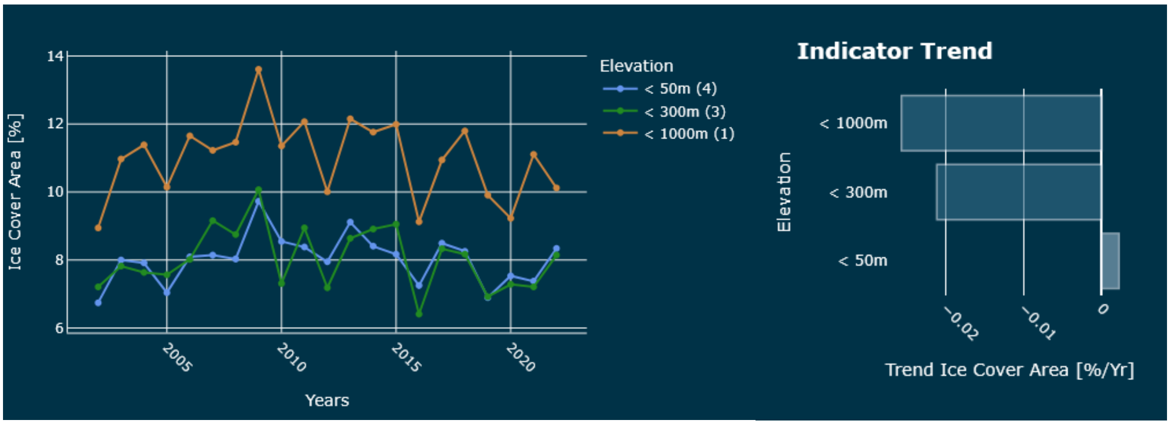


Figure 37. Time series and trends of ice cover area in Greenland aggregated by lake elevation.

### 6.3.3.2 Heat stress on lakes in China

The dashboard illustrates an increase in the frequency of heatwaves affecting Chinese lakes over the period 2002 to 2022. This upward trend is evident across all lake size categories, with a particularly sharp rise observed in the most recent years.

Trend analysis in Figure 38 reveals that the number of heatwave days has increased consistently for lakes of all surface area classes. Medium to large lakes (300–1000 km²) show an average increase of approximately 0.15 heatwave events per year, which translates to 1.5 additional heatwave days per decade. These findings are in alignment with surface air temperature trends derived from global climate datasets, such as the World Bank's Climate Change Knowledge Portal (Figure 38). Notably, both the lake-based heatwave indicator and surface air temperature datasets reflect a cooler phase around 2011 and 2012, during which fewer heatwave events were recorded. This consistency across independent datasets supports the reliability of the observed patterns.

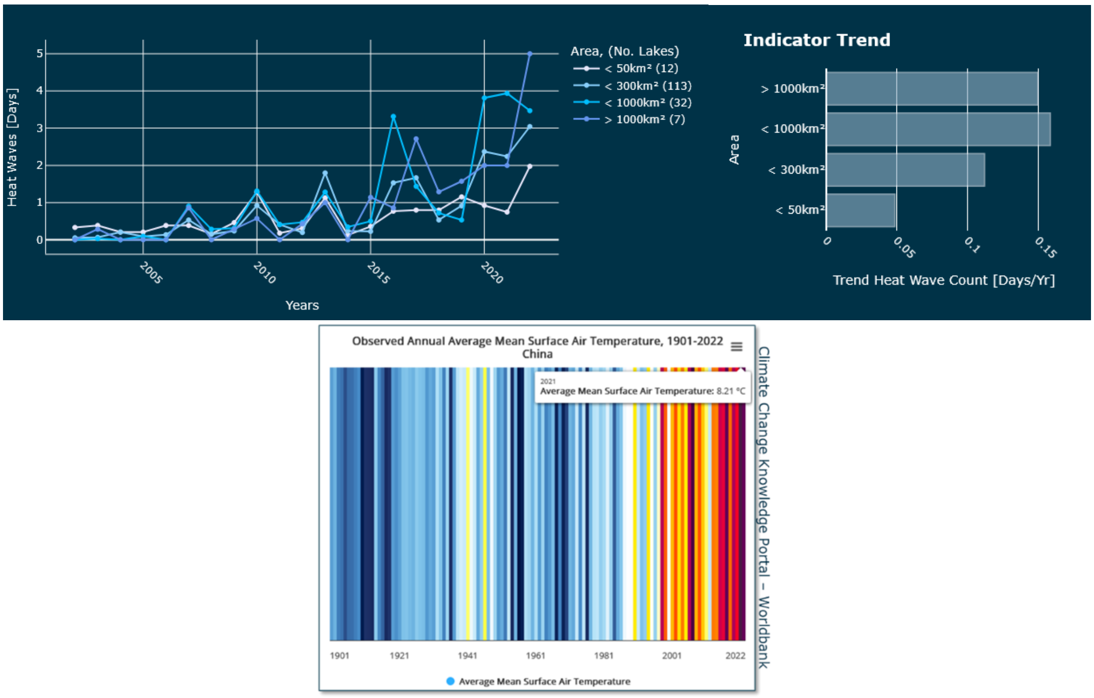


**Figure 38. Time series and Trends of heat waves in Chinese Lakes aggregated by lake area. Climate Change Knowledge Portal by Worldbank – Surface Air Temperature in China from 1901-2022.**

### 6.3.3.3 Ice Cover Duration in Sweden

The dashboard demonstrates a decreasing trend in lake ice cover duration across Sweden. This reduction is evident across lakes at all elevation levels, with the highest changes observed in lowland lakes.

Notably, lakes situated at lower altitudes exhibit a consistent decline in ice cover duration, with the trend partly driven by anomalously short ice seasons during the years 2014 and 2015. Trend analysis indicates that low-altitude lakes are experiencing a decrease in ice cover duration of up to 2 days per year. In contrast, lakes located at higher elevations (above 1000 m) generally exhibit longer periods of ice cover (Figure 39).

These findings in the dashboard are consistent with those presented in Hallerbäck et al. (2022), which is based on ground-based observational data, further supporting the observed trends.

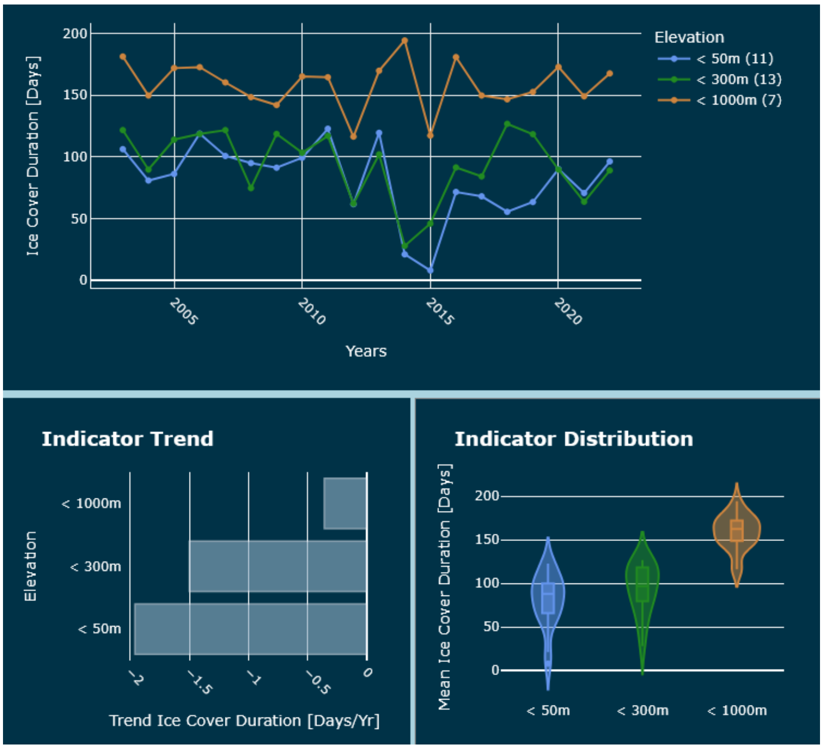


Figure 39. Time series and Trends of ice cover duration in Swedish lakes aggregated by elevation levels.

# 7 External studies review

This final section presents an update based on more recent external scientific studies (limited to 2025) with respect to the last URD v3.0.1, using the Lakes_cci dataset. In particular, two studies were found:

- Kangro et al. (2025) used Chl-a, LSWT, LWL to assess phytoplankton bloom dynamics in the shallow, eutrophic Lake Peipsi (Estonia);
- Bonnier et al. (2024) investigated lake water quality in Lake Geneva, with particular focus on phytoplankton abundance and phenology from Chl-a concentrations.

A few more studies referring to CCI data were also found but, although focusing on lakes, they have been supported by the Ocean Colour CCI (OC-CCI) project. In particular, Binding et al. (2024) used OC-CCI products for reporting on water clarity status and long-term trends in North America's largest lakes. Extensive matchups between the OC-CCI $K_d$ at 490 nm ($K_d$ 490 enabled robust multi-lake validation of Secchi disk depth - $Z_{SD}$) and in situ $Z_{SD}$ observations spanning 25 years retrievals over a wide range of water clarity conditions. Nezlin et al. (2025) performed a detailed analysis of Chl-a spatial and temporal patterns of freshwater ecosystems within the Laurentian Great Lakes from the OC-CCI dataset. They analysed 25 years (1997–2022) of monthly composites covering most of the Great Lakes area detecting regime shifts in Chl-a. Kutser and Soomets (2024) conducted a study in large lakes to investigate changes in Chl-a, particulate matter ($b_{bp}(555)$) and coloured dissolved organic matter CDOM ($a_{dg}(412)$) in the Caspian Sea and in ten next largest lakes over the 1997–2023 period, from OC-CCI. One benefit of the OC-CCI dataset compared to Lakes_cci is its use of band-shifting to harmonise observations from the whole observation period, using additional sensors. However, work presented by Lakes_cci shows that, outside of the largest lakes, sensors such as MODIS are not well suited to consistently determine lake optical properties (Liu et al. 2024).

# 8 Conclusions

This report presents an in-depth exploration of the Lakes_cci Climate Research Data Package (CRDP) v2.1.0, offering a global overview of data distribution. Distribution plots illustrate the range of variation across key variables. Data extraction followed the recommendations and best practices outlined in the Product User Guide (PUG) and Product Specification Document (PSD), including the application of uncertainty metrics and quality flags, hence indicating the value of both documents.

Analyses and assessments featured in this report highlight diverse applications of the Lakes_cci dataset at both continental and global scales, supplemented by selected regional case studies (e.g., Lake Qadisiyah, Iraq). The studies explore individual and combined Essential Climate Variables (ECVs) such as water colour, Chl-a, LSWT, turbidity, and water level. Additionally, newly developed climate indicators—including LSWT anomaly, heatwaves, ice cover, and the recently introduced ice duration—were applied to reveal geographical patterns of change. At the global level, a preliminary assessment of long-term trends in water colour, Chl-a, and turbidity across 2024 lakes demonstrated for the first time the potential of the Lakes_cci dataset to monitor global-scale changes in lake water quality. At the continental scale, a subset of African lakes was selected to capture a range of geographical sub-regions, morphometric features, and trophic states. A preliminary analysis of time series patterns was conducted using LSWT, Chl-a and turbidity in conjunction with meteo-climatic data. This enabled the identification of compound extreme events and the investigation of lake-specific responses.

This document also summarizes the results of selected project use cases. Notably, the Lakes_cci data were used to assess lake responses to the 2019 European and Indian heatwaves, revealing both continental-scale patterns and specific morphological responses. In India, a strong correlation between turbidity and monsoon rainfall was observed. In a detailed case study of Lake Qadisiyah (Iraq), located in a hot desert climate, long-term changes in LWL, Chl-a, and turbidity were analysed to evaluate the influence of La Niña on both water quantity and quality. Furthermore, at a global scale, joint analysis of water level (quantity) and turbidity (quality) revealed complex seasonal and interannual relationships. Finally, the report showcases new functionalities of the Climate Indicators Dashboard and demonstrates the practical application of these indicators across various regions.

Several scientific publications have resulted from this project and its datasets (see the project website, https://climate.esa.int/en/projects/lakes/). The review of publications showed that the Lakes_cci dataset is starting to be used by a wider community of researchers for lake studies. However, more outreach work seems needed, as some groups are using different CCI datasets.

A summary of evolving user requirements is available in the most recent User Requirement Document (URD) v3.0.1. This report therefore focuses on summarizing and updating recent external studies that have applied the Lakes_cci dataset.

During this second phase of the project, efforts focused on exploring the value of this unique dataset and highlighting its potential. We actively promoted the dataset by participating in conferences, preparing scientific manuscripts, and engaging with various user communities.

# 9 References


Barlow, M., Zaitchik, B., Paz, S., Black, E., Evans, J., & Hoell, A. (2016). A review of drought in the Middle East and southwest Asia. Journal of climate, 29(23), 8547-8574.

Calamita, E., Lever, J.J., Albergel, C., Woolway, R.I. and Odermatt, D. (2024) Detecting climate-related shifts in lakes: A review of the use of satellite Earth Observation. Limnol Oceanography, https://doi.org/10.1002/lno.12498

Camuffo, D., Becherini, F., & Della Valle, A. (2020). Relationship between selected percentiles and return periods of extreme events. Acta Geophysica, 68(4), 1201–1211.

Caroni, R.; Pinardi, M.; Free, G.; Stroppiana, D.; Parigi, L.; Tellina, G.; Bresciani, M.; Albergel, C.; Giardino, C. (2024) Investigating the Impact of Wildfires on Lake Water Quality Using Earth Observation Satellites. Appl. Sci., 14, 2626. https://doi.org/10.3390/app14062626

Carrea, L., C.J. Merchant, R.I. Woolway et al (2024), Lake surface water temperature [in State of the Climate Report] in Bulletins of the American Meteorological Society. 105 (8), S33-S35, https://doi.org/10.1175/BAMS-D-24-0116.1

Carrea, L., Crétaux, J. F., Liu, X., Wu, Y., Calmettes, B., Duguay, C. R., ... & Albergel, C. (2023). Satellite-derived multivariate world-wide lake physical variable time series for climate studies. Scientific Data, 10(1), 30.

Cocquyt, C., Plisnier, P. D., Mulimbwa, N. S., & Nshombo, M. (2021). Unusual massive phytoplankton bloom in the oligotrophic Lake Tanganyika. Plant Ecology and Evolution, 154(3), 351-361.

Codjoe, S. N. A., & Atiglo, D. Y. (2020). The Implications of Extreme Weather Events for Attaining the Sustainable Development Goals in Sub-Saharan Africa. Frontiers in Climate, 2, Article 592658.

Copernicus Climate Change Service (2023). ERA5 hourly data on single levels from 1940 to present. ECMWF. https://cds.climate.copernicus.eu/cdsapp#!/dataset/reanalysis-era5-single-levels?tab=overview https://doi.org/10.24381/cds.adbb2d47

Daham, A., Han, D., Rico-Ramirez, M., & Marsh, A. (2018). Analysis of NVDI variability in response to precipitation and air temperature in different regions of Iraq, using MODIS vegetation indices. Environmental Earth Sciences, 77(10), 1-24.

Digital Earth Africa (2022). ESA Climate Change Initiative Land Cover: 1992-2019. https://explorer.digitalearth.africa/products/cci_landcover

Dörnhöfer, K., & Oppelt, N. (2016). Remote sensing for lake research and monitoring–Recent advances. Ecological Indicators, 64, 105-122.

Duncombe, J. (2019), Greenland ice sheet beats all-time 1-day melt record, Eos, 100, https://doi.org/10.1029/2019EO130349. Published on 02 August 2019.

ESA (2017). Land Cover CCI Product User Guide Version 2. Tech. Rep. Available at: maps.elie.ucl.ac.be/CCI/viewer/download/ESACCI-LC-Ph2-PUGv2_2.0.pdf

Free, G., Bresciani,M., Pinardi,M., Simis,S., Liu,X., Albergel, C., Giardino,C. (2022). Investigating lake chlorophyll-a responses to the 2019 European double heatwave using satellite remote sensing, Ecological Indicators, 142, 109217, https://doi.org/10.1016/j.ecolind.2022.109217.

Giardino, C., Brando, V. E., Gege, P., Pinnel, N., Hochberg, E., Knaeps, E., ... & Dekker, A. (2019). Imaging spectrometry of inland and coastal waters: state of the art, achievements and perspectives. Surveys in Geophysics, 40, 401-429.

Greife A.J., 2023. Evaluation of water quality changes in African lakes in response to climate trends and extreme events based on satellite and meteo-climatic data. Master Degree Thesis in Environmental Change and Global Sustainability.

Hallerbäck, S., Huning, L. S., Love, C., Persson, M., Stensen, K., Gustafsson, D., & AghaKouchak, A. (2022). Climate warming shortens ice durations and alters freeze and break-up patterns in Swedish water bodies. The Cryosphere, 16(6), 2493-2503.

Hari, M., & Tyagi, B. (2021). Investigating Indian summer heatwaves for 2017–2019 using reanalysis datasets. Acta Geophysica, 69(4), 1447-1464.

Hasan, M., Moody, A., Benninger, L., & Hedlund, H. (2019). How war, drought, and dam management impact water supply in the Tigris and Euphrates Rivers. Ambio, 48, 264-279.

Havens, K., Paerl, H., Phlips, E., Zhu, M., Beaver, J., & Srifa, A. (2016). Extreme Weather Events and Climate Variability Provide a Lens to How Shallow Lakes May Respond to Climate Change. Water, 8(6), 229.

Hersbach, H., Bell, B., Berrisford, P., Hirahara, S., Horányi, A., and Muñoz-Sabater, J. (2020). The ERA5 global reanalysis. Quarterly Journal of the Royal Meteorological Society 146(730), 1999–2049.

Hobday, A. J., Alexander, L. V., Perkins, S. E., Smale, D. A., Straub, S. C., Oliver, E. C., ... & Wernberg, T. (2016). A hierarchical approach to defining marine heatwaves. Progress in Oceanography, 141, 227-238.

IPCC (2014). Climate change 2014: Synthesis Report: Mach KJ, Meyer LA, Pachauri RK, Planton S, von Stechow C (eds) Annex II: Glossary. Contribution of Working Groups I, II and III to the Fifth Assessment Report of the Intergovernmental Panel on Climate Change. Geneva. IPCC. https://www.ipcc.ch/report/ar5/syr/.

Jeppesen, E., Pierson, D., & Jennings, E. (2021). Effect of Extreme Climate Events on Lake Ecosystems. Water, 13(3), 282. https://doi.org/10.3390/w13030282.

Jiang Dalin, Ian Jones, Xiaohan Liu, Stefan G.H. Simis, Jean-François Cretaux, Clement Albergel, Andrew Tyler, Evangelos Spyrakos. (2024) Impacts of droughts and human activities on water quantity and quality: Remote sensing observations of Lake Qadisiyah, Iraq. International Journal of Applied Earth Observation and Geoinformation, Volume 132, 2024, 104021, ISSN 1569-8432. https://doi.org/10.1016/j.jag.2024.104021

Kamnev, N. M., Sonichev, N. A., & Malyshev, N. A. (1983). Earth dam of the Al-Hadithah hydropower development on the Euphrates River. Hydrotechnical Construction, 17(10), 530-533.

Khan, S. J., Deere, D., Leusch, F. D. L., Humpage, A., Jenkins, M., & Cunliffe, D. (2015). Extreme weather events: Should drinking water quality management systems adapt to changing risk profiles? Water Research, 85, 124–136.

Khazaei, B., Read, L. K., Casali, M., Sampson, K. M., & Yates, D. N. (2022). Globathy, the global lakes bathymetry dataset. Scientific Data, 9(1), 36.

Lehmann, M. K., Nguyen, U., Allan, M., & Van der Woerd, H. J. (2018). Colour classification of 1486 lakes across a wide range of optical water types. Remote Sensing, 10(8), 1273.

Liu Xiaohan, Warren Mark, Selmes Nick, Simis Stefan G.H. (2024) Quantifying decadal stability of lake reflectance and chlorophyll-a from medium-resolution ocean color sensors. Remote Sensing of Environment, Volume 306, 2024, 114120, ISSN 0034-4257. https://doi.org/10.1016/j.rse.2024.114120.

Lomeo D., S. G.H. Simis, X. Liu, N. Selmes, M. A. Warren, A. D. Jungblut, E. J. Tebbs. (2025) A novel cyanobacteria occurrence index derived from optical water types in a tropical lake. ISPRS Journal of Photogrammetry and Remote Sensing, Volume 223, Pages 58-77, ISSN 0924-2716, https://doi.org/10.1016/j.isprsjprs.2025.03.006.

Maartje C. Korver, Bernhard Lehner, Jeffrey A. Cardille, Laura Carrea, (2024), Surface water temperature observations and ice phenology estimations for 1.4 million lakes globally. Remote Sensing of Environment, Volume 308,2024,114164,ISSN 0034-4257, https://doi.org/10.1016/j.rse.2024.114164.

Mangilli, A.; Duguay, C.R.; Murfitt, J.; Moreau, T.; Amraoui, S.; Mugunthan, J.S.; Thibaut, P.; Donlon (2024) Improving the Estimation of Lake Ice Thickness with High-Resolution Radar Altimetry Data. C. Remote Sens., 16, 2510. https://doi.org/10.3390/rs16142510

Messager, M. L., Lehner, B., Grill, G., Nedeva, I., & Schmitt, O. (2016). Estimating the volume and age of water stored in global lakes using a geo-statistical approach. Nature communications, 7(1), 13603.

Messager, M.L., Lehner, B., Grill, G., Nedeva, I., Schmitt, O. (2016). Estimating the volume and age of water stored in global lakes using a geo-statistical approach. Nature Communications, 7: 13603.

Palmer, S. C., Kutser, T., & Hunter, P. D. (2015). Remote sensing of inland waters: Challenges, progress and future directions. Remote sensing of Environment, 157, 1-8.

Piccolroaz, S., Zhu, S., Ladwig, R., Carrea, L., Oliver, S., Piotrowski, A. P.,et al. (2024). Lake Water Temperature Modeling in an Era of Climate Change: Data Sources, Models, and Future Prospects. Reviews of Geophysics,62, e2023RG000816. https://doi.org/10.1029/2023RG000816

Pitarch, J., van der Woerd, H. J., Brewin, R. J., & Zielinski, O. (2019). Optical properties of Forel-Ule water types deduced from 15 years of global satellite ocean color observations. Remote Sensing of Environment, 231, 111249.

Plisnier, P.-D., Kayanda, R., MacIntyre, S., Obiero, K., Okello, W [William], Vodacek, A., Cocquyt, C., Abegaz, H., Achieng, A., Akonkwa, B., Albrecht, C., Balagizi, C., Barasa, J., Abel Bashonga, R., Bashonga Bishobibiri, A., Bootsma, H., Borges, A. V., Chavula, G., Dadi, T., . . . Lawrence, T. (2022). Need for harmonized long-term multi-lake monitoring of African Great Lakes. Journal of Great Lakes Research, 101988.

Ranasinghe, R., Ruane, A.C., Vautard, R., et al., 2021. Chapter 12: Climate change information for regional impact and for risk assessment. Climate Change 2021: The Physical Science Basis. Contribution of Working Group I to the Sixth Assessment Report of the Intergovernmental Panel on Climate Change. Cambridge University Press.

Ratnam, J.V., Behera, S.K., Ratna, S.B., Rajeevan, M. and Yamagata, T. (2016) Anatomy of Indian heatwaves. Scientific Reports, 6, 24395.

Rohini, P., Rajeevan, M. & Srivastava, A. K. (2016) On the variability and increasing trends of heat waves over India. Sci. Rep., 6,1–9.

Shen, Q., Friese, K., Gao, Q., Yu, C., Kimirei, I. A [Ismael A.], Kishe-Machumu, M. A., Zhang, L [Lu], Wu, G., Liu, Y [Yuanbo], Zhang, J [Jiaqi], Mgana, H., Dadi, T., Mpanda, D. W., & Chen, S. S. (2022). Status and changes of water quality in typical near-city zones of three East African Great Lakes in Tanzania. Environmental Science and Pollution Research International, 29(23), 34105–34118.

Shen, X., Ke, C. Q., Duan, Z., Cai, Y., Li, H., & Xiao, Y. (2025). Satellite observations reveal widespread color variations in global lakes since the 1980s. Water Resources Research, 61(1), e2023WR036926.

Sousa, P. M., Barriopedro, D., García-Herrera, R., Ordóñez, C., Soares, P. M., & Trigo, R. M. (2020). Distinct influences of large-scale circulation and regional feedbacks in two exceptional 2019 European heatwaves. Communications Earth & Environment, 1(1), 48.

Spyrakos, E., O'donnell, R., Hunter, P. D., Miller, C., Scott, M., Simis, S. G., ... & Tyler, A. N. (2018). Optical types of inland and coastal waters. Limnology and Oceanography, 63(2), 846-870.

Sylvestre. F., A. Mahamat-Nour, T. Naradoum, M. Alcoba, L. Gal, A. Paris, J-F. Cretaux, B. Pham-Duc, M. Mahamat Ahmat, D. Gaya. (2024) Strengthening of the hydrological cycle in the Lake Chad Basin under current climate change Nat. Geosci. 17, 516–523 (2024). https://doi.org/10.1038/s41561-024-01446-w

Tarnavsky, E., Grimes, D., Maidment, R., Black, E., Allan, R. P., Stringer, M., Chadwick, R., & Kayitakire, F. (2014). Extension of the TAMSAT Satellite-Based Rainfall Monitoring over Africa and from 1983 to Present. Journal of Applied Meteorology and Climatology, 53(12), 2805–2822. https://doi.org/10.1175/JAMC-D-14-0016.1.

UNEP. (2017). Environmental issues in areas retaken from ISIL: Mosul, Iraq. Technical report, rapid scoping mission, July – August 2017.

Vittal, H., Villarini, G., & Zhang, W. (2020) On the role of the Atlantic ocean in exacerbating Indian heat waves. Climate dynamics, 54(3), 1887-1896.

Vollenweider, R. A., & Kerekes, J. (1982). Eutrophication of waters. Monitoring, assessment and control. Organization for Economic Co-Operation and Development (OECD), Paris, 156.

Winton, R. S., Teodoru, C. R., Calamita, E., Kleinschroth, F., Banda, K., Nyambe, I., & Wehrli, B. (2021). Anthropogenic influences on Zambian water quality: Hydropower and land-use change. Environmental Science. Processes & Impacts, 23(7), 981–994.

Woolway, R. I., Jennings, E., Shatwell, T., Golub, M., Pierson, D. C., & Maberly, S. C. (2021). Lake heatwaves under climate change. Nature, 589(7842), 402-407.

Yang, H., Kong, J., Hu, H., Du, Y., Gao, M., & Chen, F. (2022b). A review of remote sensing for water quality retrieval: Progress and challenges. Remote Sensing, 14(8), 1770.

Yang, X., O'Reilly, C. M., Gardner, J.R., Ross, M. R. V., Topp, S. N., Wang, J., & Pavelsky, T. M. (2022a). The color of Earth's lakes. Geophysical Research Letters, 49, e2022GL098925. https://doi.org/10.1029/2022GL098925.

Zeman-Kuhnert, S., Thiel, V., & Heim, C. (2022). Effects of Weather Extremes on the Nutrient Dynamics of a Shallow Eutrophic Lake as Observed during a Three-Year Monitoring Study. Water, 14(13), 2032.

Zhang, R., Sun, C., Zhu, J., Zhang, R., & Li, W. (2020). Increased European heat waves in recent decades in response to shrinking Arctic sea ice and Eurasian snow cover. NPJ Climate and Atmospheric Science, 3(1), 7.

Zore, T., Landu, K., Gogoi, P. P. & Vinoj, V. (2021) Effect of tropical sub-seasonal variability on heatwaves over India. Int J Climatol., 41 (Suppl. 1): E2258–E2268.

# 10 Appendix

## Appendix A 1 -

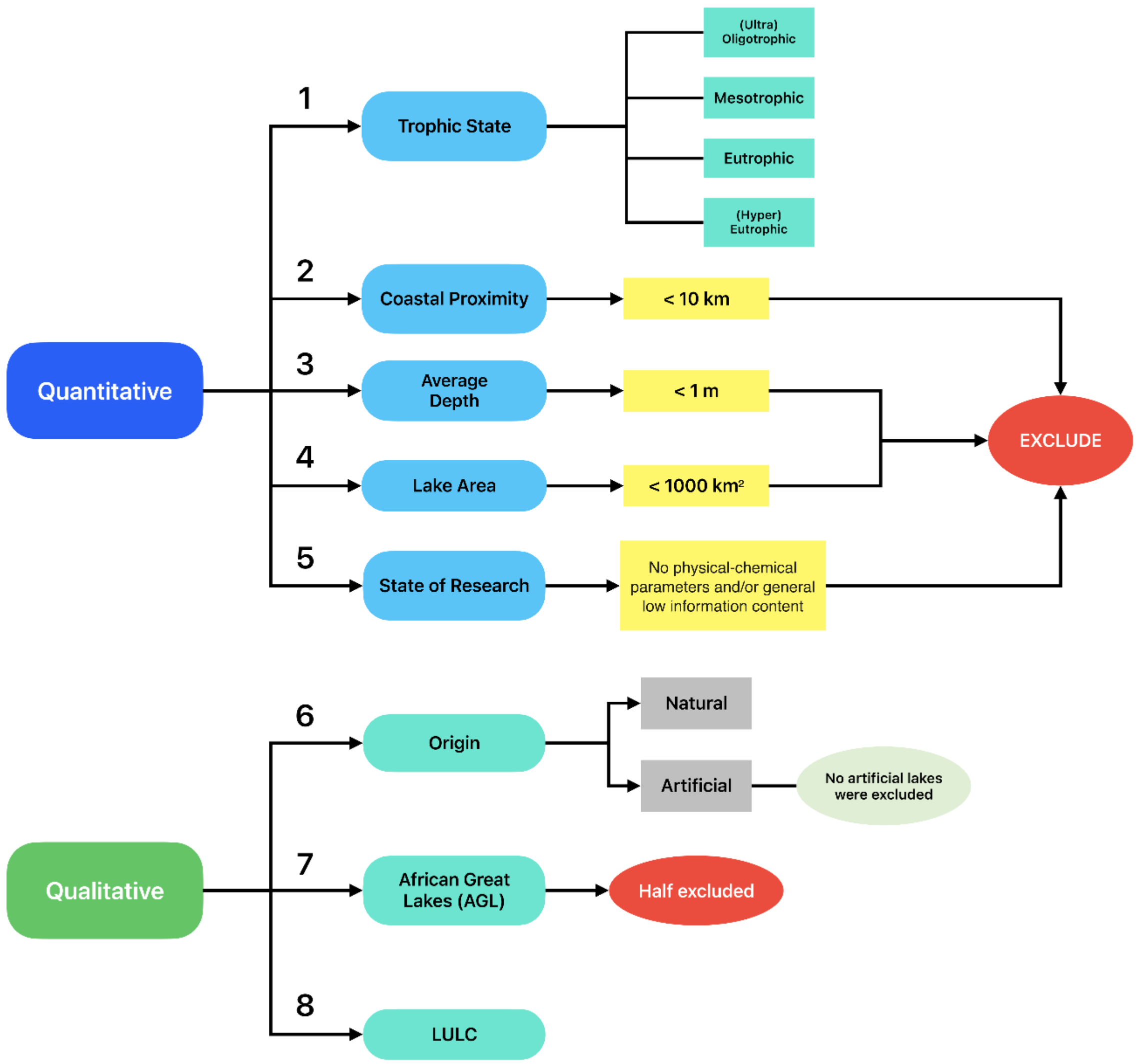


Figure 40: Schematic workflow of the lake selection including selection criteria and their threshold where applicable.

# Appendix A 2 -

Table A1. List of lakes included in the analysis of the India-Pakistan sub-continental region, as showed in Figure 22.

| Lake_ID | Lake_Name |
|---|---|
| 204 | Chilika |
| 249 | Hirakud |
| 289 | Srisailam |
| 347 | Gandhi |
| 442 | Govind Ballabah Pant |
| 463 | Pulicat |
| 498 | Nagarjuna |
| 528 | Tungabhadra |
| 563 | Vembanad |
| 622 | Maharana Pratap |
| 937 | Rana Pratap |
| 1059 | Ukai |
| 1149 | Rann-Of-Kutch |
| 1219 | Nath |
| 1302 | Tso-Moriri |
| 1501 | Matatila |
| 2923 | Manchar |
| 300001398 | Tarbela |
| 300001496 | Narmada |
| 300001497 | Hasdeo Bango |
| 300001503 | Rengali |
| 300001508 | Indravati |
| 300001509 | Sriram |
| 300015361 | Ramganga |
| 300015502 | Rajghat |
| 300015520 | Masanjore |
| 300015523 | Dharoi |
| 300015536 | Mahi Bajaj |
| 300015538 | Halali |
| 300015552 | Barna |
| 300015554 | Chandil |
| 300015557 | Nalsarovar |
| 300015606 | Upper Wardha |
| 300015630 | Madhuban |
| 300015638 | Isapur |
| 300015650 | Majalgaon |
| 300015672 | Lower Manair |
| 300015697 | Yeleru |
| 300015714 | Jurala |
| 300015736 | Supa |

| | |
|---|---|
| 300015761 | Bhadra |
| 300015811 | Bhavani |